Master Thesis

Microstructural and heat treatment investigations of aluminium alloy type Al-Mg-Zn-Cu produced by wire arc additive manufacturing

Carried out for the purpose of obtaining the degree Dipl.-Ing., submitted at TU Wien, Faculty of Mechanical and Industrial Engineering, by

Ehsan GHANBARI
Mat.Nr. 1127821

Under the supervision of
Univ. ASS. Dipl.-Ing. Dr. techn. Ahmad Falahati
And
Univ. Prof. Dipl.-Ing. Dr. techn. Ernst Kozeschnik

E308
Institute of Materials Science and Technology

Vienna, April 2020 Signature

Abstract

One of the important properties of the aluminium alloy 7xxx series is their high response to the age hardening. A new produced alloy with higher amount of Mg than Zn with chemical composition of Al-3.5Zn-5Mg-0.3Cu (wt%), which was produced by Wire Arc Additive Manufacturing (WAAM) is investigated to find the effect of different aging conditions on the hardening behaviour of the alloy.

The mechanical property is characterized by hardness measurements. Single step aging and two-step aging with pre-aging were performed to measure the hardness values.

The optimized aging with the highest hardness is found to be a two–step aging, after solution treatment and quenching of the alloy. Artificial aging to 90°C for 24 hours and then aging for 622 hours at 140°C showed significantly improved hardness in compare to single step-aging cycles at 90°C and 140°C.

Differential scanning calorimetry (DSC) was used to record precipitation and dissolution reactions from 25°C to 500 °C. The measurements were executed for different heating rates.

In this work, the crystal structures of the formed precipitates were investigated by transmission electron microscopy (TEM) and high-resolution transmission electron microscopy (HRTEM). TEM investigations show hardness improvement in the Al-3.5Zn-5Mg-0.3Cu alloy is mainly due to the formation of fine and homogeneously distributed metastable T-$Mg_{32}(AlZn)_{49}$ phase (or T´-phase) in the aluminium matrix.

Kurzfassung

Eine der wichtigen Eigenschaften der Aluminiumlegierung der Serie 7xxx ist ihre starke Reaktion auf die Aushärtung.

Eine mittels Wire Arc Additive Manufacturing (WAAM) neu hergestellte Legierung, die einen höheren Anteil von Mg als Zn besitzt und eine chemischen Zusammensetzung von Al-3.5Zn-5Mg-0.3Cu (wt%) aufweist, wurde untersucht um den Effekt verschiedener Auslagerungszustände auf die Härteverhältnisse der Legierung herauszufinden.

Die mechanische Eigenschaft wurde durch Härtemessungen beschrieben. Sowohl eine einstufige Auslagerung als auch eine zweistufige Auslagerung mit einer Vorauslagerung wurden durchgeführt, um die Härtewerte zu messen.

Die optimale Auslagerung mit der stärksten Härte nach Lösungsglühen und Abschrecken der Legierung ist die zweistufige Auslagerung. Somit zeigte sich, dass eine Warmauslagerung auf 90°C für 24 Stunden und eine anschließende Auslagerung auf 140°C für 622 Stunden eine signifikant verbesserte Härte im Vergleich zu einer nur einstufigen Auslagerung bei 90°C beziehungsweise 140°C aufweist.

Differential Scanning Calorimetry (DSC) wurde verwendet, um die Ausscheidungs- und Auflösungsreaktion bei 25°C bis 500°C aufzuzeichnen. Die Messungen wurden bei unterschiedlichen Heizraten durchgeführt.

In dieser Diplomarbeit wurden die Kristallstrukturen der gebildeten Ausscheidungen mittels Transmission Electron Microscopy (TEM) und High Resolution Transmission Electron Microscopy (HRTEM) untersucht.

Die TEM-Untersuchungen zeigen, dass die Verbesserung der Legierungshärte von Al-3.5Zn-5Mg-0.3Cu hauptsächlich auf die Bildung einer fein und homogen verteilten metastabilen T-Mg_{32} $(AlZn)_{49}$ Phase beziehungsweise T´- Phase in der Aluminiummatrix zurückzuführen ist.

Acknowledgements

I would like to thank in particular Dr. Falahati for giving me the opportunity for doing this thesis to expand my knowledge in the field of aluminium alloys and also for supporting me during my work, and I have to thank Prof. Kozeschnik, head of the Institute of Materials Science and Technology TU Wien, for the supervision of this thesis.

Sincere thanks to Dr. Piotr Warczok, who helped me through my thesis.

I have to thank Tomasz Wojicik for sharing his knowledge with me and carrying out the TEM investigation and evaluation of the TEM images. I also want to thank the USTEM team for TEM sample preparation.

I like to thank Edith Asemio, Kurt Caloun and Stefan Zellhofer for supporting me in the laboratory and sharing their knowledge with me.

Finally, special thanks to my family and my wife, Zahra, who always encouraged and supported me during these years to achieve my goals.

Table of contents

1 Introduction 1

2 Objectives 2

3 State of the art 3

3.1 Additive Manufacturing Process 3

3.1.1 Classification of Additive Manufacturing Processes 3

3.2 Classification of Aluminium alloy 7

3.3 Alloy strengthening mechanisms 9

3.3.1 Solid solution strengthening 9

3.3.2 The precipitation hardening strengthening 10

3.3.3 The related phases sequences to the produced alloy 17

4 Experimental 19

4.1 Material 19

4.2 Heat treatment 21

4.3 Metallography 23

4.4 Differential Scanning Calorimetry (DSC) Measurements 24

4.4.1 Samples preparation 24

4.4.2 Heat treatment sequence 24

4.5 Hardness Measurements 26

4.5.1 Sample Heat treatment 26

4.6 TEM Investigation 27

4.6.1 Sample preparation 27

5 Results 28

5.1 Metallography 28

5.2 DSC Measurements 29

5.2.1 Calculating onset melting points of the alloys 29

5.2.2 DSC results for the alloy from T4 condition with different heating rates 30

5.3 Hardness Measurements 31

5.4 TEM Investigation 32
5.4.1 TEM investigation for sample (1) 33
5.4.2 TEM investigation for sample (2) 36
5.4.3 TEM investigation for sample (3) 40
6 Discussion 44
6.1 Comparison of different heat treatment conditions on hardness of the alloy 44
6.2 Differential Scanning Calorimetry (DSC) 45
6.3 Comparison of TEM results for different heat treatment condition 47
7 Summary and Conclusions 49
8 References 50
9 List of figures 52
10 List of tables 54

1 Introduction

7xxx aluminium alloys (Al-Zn-Mg-Cu) offer very high strength, due to the high response to the precipitation hardening.

The principal alloying element of conventional 7xxx series are Zn with higher wt% among other adding elements. In the new designed alloy, Al- 3.5 Zn- 5 Mg- 0.3 Cu (wt %), which is subject of our study, Mg is available in higher concentration than Zn.

The alloy is produced using the Gas Metal Arc Welding (GMAW) based on process of Cold Metal Transfer (CMT). This unique method enables fabrication of the structure in a layer-by-layer manner.

The same as the alloys 7xxx-series, the new designed alloy is age-hardenable, it can be strengthened by heat treatment processes. The strength of the material will be achieved by formation of fine metastable precipitates. The precipitation sequence of the alloy during different aging conditions and the microstructure of the formed precipitates, which resist against dislocation movements and cause to increase mechanical properties, is subject of our investigations.

2 Objectives

The focus of this thesis is on characterisation of a new produced aluminium alloy, which is produced by wire-arc additive manufacturing (WAAM) with chemical composition of Al-3.5Zn-5Mg-0.3Cu (wt%). The alloying elements are similar to the 7xxx series; however, in the new designed alloy the amount of Mg is higher than Zn, which make it different as conventional available 7xxx series. The new chemical composition and unique production process of the alloy may affect the properties of material. Therefore, the investigations of the achieved properties are in demand.

The goal of this thesis is to investigate the effects of different heat treatment conditions on precipitation hardening behaviour and on hardness of the Al-3.5Zn-5Mg-0.3Cu alloy by formation of the metastable precipitates, during aging conditions.

The microstructure and crystal structure of the formed precipitates, which affect the mechanical properties of the material, should be investigated under TEM.

3 State of the art

This chapter gives an overview about additive manufacturing technologies and its production methods. In addition, the classification of aluminium alloys and manufactured alloy by Gas Metal Arc Welding (GMAW) process will be reviewed.

3.1 Additive Manufacturing Process

The additive manufacturing (AM) over the past 30 years becomes a key technology in recent years in the manufacturing industry. Beside CNC machining, which is a subtractive method for high quality components manufacturing with help of programming, additive manufacturing, which is additive method, creates near net shape parts directly rapid prototyping.

According standard ASTM F2792-10, AM is defined as "*The process of joining materials to make objects from 3D model data, usually layer upon layer, as opposed to subtractive manufacturing technologies*" [1].

This technology has gained more interest and attention by more flexibility, sustainability and lower costs. In compare to the traditional manufacturing processes, additive manufacturing is a reliable alternative that is cost-competitive for fabricating expensive components with complicated geometries. Additive manufacturing is possible not only for the direct formation of the metal products as a prototype, but also for producing the final products by means of automated process [2].

3.1.1 *Classification of Additive Manufacturing Processes*

For metal component, which are obtained in layer-by-layer manner, the additive manufacturing (AM) techniques can be classified according to the energy source and row material.

Metal additive manufacturing based on raw materials are divided into three groups:

- Wire-based
- Powder-based
- Sheet-based

Among these groups, wire-based is more material efficient with higher deposition rates.

Based on the energy sources, which are applied for the deposition, three groups are introduced namely:

- Arc welding-based
- Laser-based
- Electron beam-based.

Applying different energy sources for each of raw materials results in new technologies and processes.

The combination of wire-based system with different energy sources are known, respectively as WAAM (Wire and Arc Additive Manufacturing), WLAM (Wire and Laser Additive Manufacturing) and EBF (Electron Beam freeform Fabrication).

In this section Wire-Arc Additive Manufacturing (WAAM) technology will be discussed in more detail, since the manufactured alloy produced with this technology.

Arc based welding is more economical among the other energy sources (laser- and electron beam-based). Wire-Arc Additive Manufacturing (WAAM) is a modern welding process to produce components by melting welding wires. It has a potential to manufacture the parts with greatly reduced waste material in complex geometric features in compare to conventional machining processes [3]. Innovative Wire and Arc additive layer manufacture provides opportunity for automation the modern welding process that controls welding and material parameters, which are critical to the geometrical accuracy.

The WAAM process can provide high deposition rate. This issue can affect the accuracy of the final parts and mechanical performance. Selecting the proper chemical composition for the designed alloy have great effects on mechanical properties and corrosion resistance and can specifies the application of the consumable welding aluminium [3].

Depending on the applied heat sources for arc welding process, WAAM process divided into three groups:

- Gas Metal Arc Welding (GMAW)
- Gas Tungsten Arc Welding (GTAW)
- Plasma Arc Welding (PAW)

GTAW and PAW use a non-consumable tungsten electrode for welding process. While in GMAW an electric arc forms between the base metal and a consumable wire electrode to produce the weld.

In GMAW process, the electrode wire is perpendicular to the substrate or previous deposited weld metal, however the wire feed orientation in GTAW and PAW is variable, which affects the quality of the deposit and process planning [4].

In this deposition process, the consumable wire electrode is fed to the molten pool, normal to the layers under the protection of the shielding gas. Electric arc of the GMAW is depicted in Figure 1 [4] .

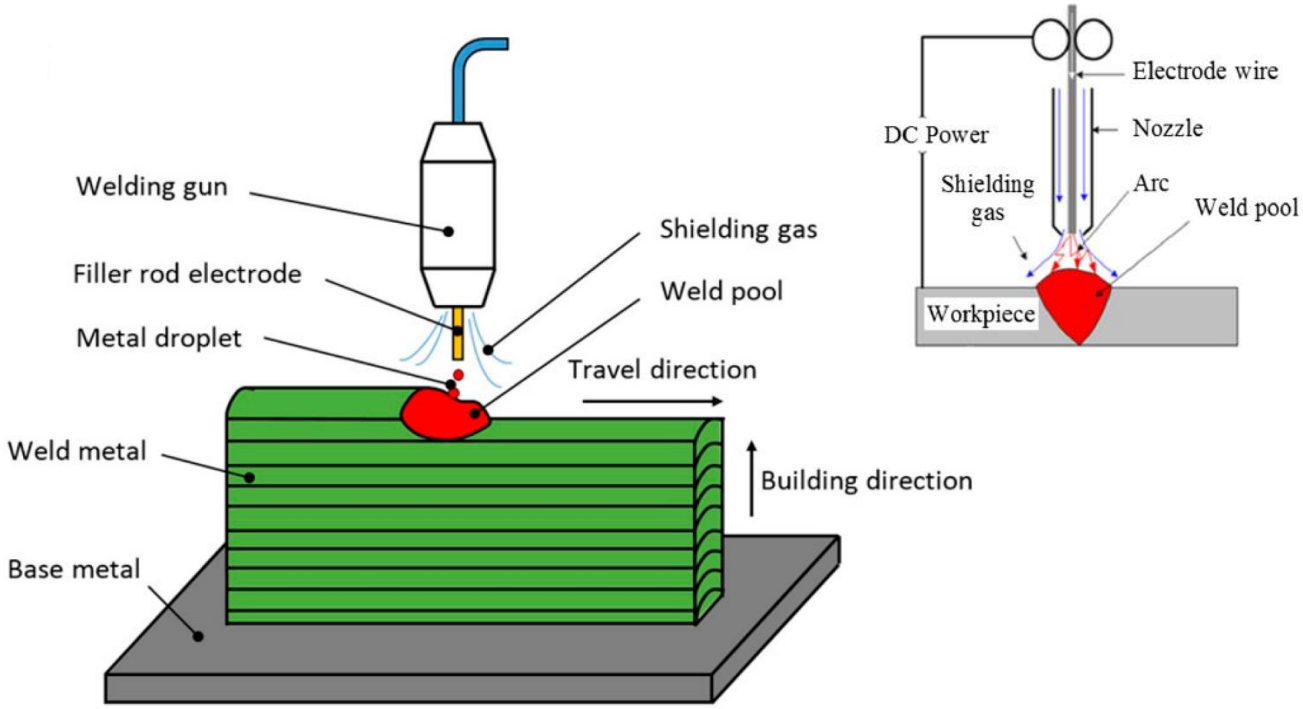

Figure 1 Schematic GMAW process layer-by-layer deposition [5] [4]

Cold Metal Transfer (CMT) is a modified GMAW process, which has been widely applied due to its high deposition rate capability and low heat input [6].

The welding process in CMT controls by a computer, which adjust the wire feed and welding speed. When the wire moves forward and dips in the molten pool, the digital control unit detects short circuit phase and a feedback signal sends to the wire feeder in order to reverse the feeding direction. By forming the arc, the wire feeder inverts the feed direction. This allow steady and precise welding, with very little spatter and slag [7].

Welding speed is also a critical for the manufacture of test pieces. Below the appropriate speed, it takes too much time for completing the process and fast welding speed leads to reducing the dimensional accuracy and surface quality of the component [8].

Beside the production process and the electrode manufacturing some properties are determinative for success of an alloy production using WAAM process [9]:

- Manufacturability of the wire (defect-free)

- Good weld-ability (droplet detachment and melt viscosity)

- Process stability (spatter-free and less susceptible to porosity)

- No / low tendency to hot cracks

- Mechanical properties according to technical requirements

- Corrosion resistance

- Melting rate

3.2 Classification of Aluminium alloy

Aluminium alloys are widely applied in the aerospace, automobile and aviation industries due to the several potentials. Easy production possibilities, good mechanical properties and formability, low density, high electrical and thermal conductivity are some of advantages of aluminium alloys.

Aluminium alloys generally divided into two groups:

- Wrought alloy
- Cast alloy

According to whether the alloy responds to heat treatment, aluminium alloys classified into two groups. The first group of alloys respond to heat treatment process by strengthening, which is known as heat treatable alloy. The other group which heat treatment has no effect on the strength of the alloys is called non-heat treatable alloy [10] [11].

This thesis deals with heat treatable wrought aluminium alloy therefore cast alloys and non-heat treatable wrought alloys are not discussed.

In Figure 2, the principle adding elements for each series of wrought aluminium alloys are presented. Among wrought aluminium alloys, series 2xxx, 6xxx and 7xxx respond to heat treatment process by strengthening.

Alloy	Main alloying element
1*xxx*	Mostly pure aluminum; no major alloying additions
2*xxx*	Copper
3*xxx*	Manganese
4*xxx*	Silicon
5*xxx*	Magnesium
6*xxx*	Magnesium and silicon
7*xxx*	Zinc
8*xxx*	Other elements (e.g., iron and silicon)
9*xxx*	Unassigned

Figure 2 Main alloying elements in wrought alloy

Among heat treatable wrought aluminium series, 7xxx alloys offer the highest strength of all aluminium alloys.7xxx series are strengthened by precipitation hardening mechanism.

This series divided into two groups:

- Aluminium -Zinc-Magnesium (Al-Zn-Mg)
- Aluminium -Zinc-Magnesium-Copper (Al-Zn-Mg-Cu)

Aluminium-Zinc in combination of magnesium Mg and copper Cu are widely used in construction material and aerospace structures.

The 7xxx of first group obtain good resistance to corrosion, however, the second group with higher amount of copper as adding elements exhibits reduced corrosion resistance [12].

The second group of alloys have the highest strengths. The alloys with higher amount of copper can be aged for higher temperatures without excessive loss of strength [13].

The 7xxx series alloys with higher amount of copper content being used in overaged T7 temper as this temper provides good resistance to exfoliation and stress corrosion cracking and maintain better combination of strength and corrosion resistance for higher aging temperatures. The 7xxx alloys however copper is often added to improve SCC resistance [12].

These alloys are strengthened by precipitation of solute-rich zones and are among the highest strength available materials based on strength-to-weight ratios [13].

3.3 Alloy strengthening mechanisms

Generally, the strength of the material increases by hindering the movement of dislocations. The real crystal lattice of a material contains dislocations. When dislocations move easily through lattice structure, material tends to be soft. By Impending the movement of dislocations, the stress required to move the dislocations increases and mechanical properties of material such as strength and hardness improve significantly [14].

In this chapter, some strengthening mechanisms regarding to wrought heat treatable alloy and the effects of heat treatment process on age-hardenable alloys will be explained.

3.3.1 *Solid solution strengthening*

One of the strengthening mechanisms, which increase the strength of material to resist against dislocation movements, is solid solution strengthening. In this mechanism, the alloying elements atoms (solute) form solid solution by dissolving in the lattice of base metal (solvent) to increase the strength of the material.

The alloying elements by locating interstitial or substitutional to crystal structure create strain field, which interacts with gliding dislocations.

The solute atoms, which position within a gap in the crystal structure of the pure metal, form interstitial solid solution. The crystal structure is then distorted as showed in Figure 3.The distorted crystal structure form local strain field, which acts as a barrier to the dislocation movements. In interstitial solid solution, the size of solute atoms are usually larger than interstitial voids that they occupy. Interstitial solid solution strengthening is normally not considered for aluminium alloys.

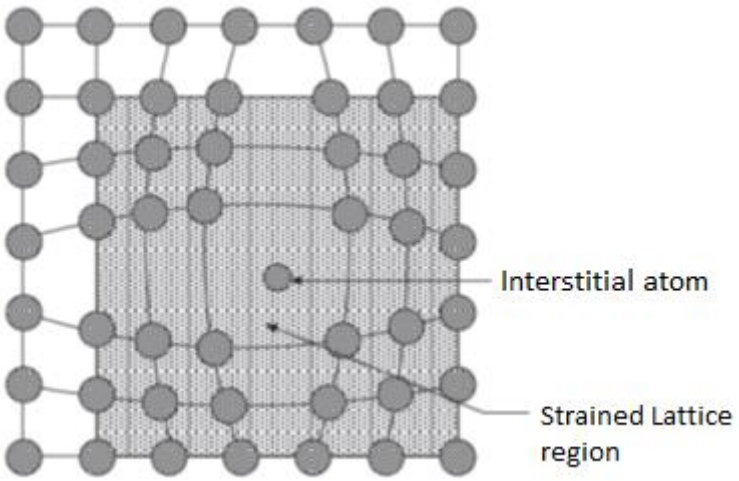

Figure 3 Interstitial solid solution and high strained region within the crystal structure [14]

Alloying element atoms, which are replaced with the base metal atoms within the crystal structure, are known as substitutional solid solutions. According to the atomic size difference between the solute and solvent atoms, the created strain field is tensile when the alloying element atoms is smaller than the solvent atoms, Figure 4 (a) and is compressive when the solute atoms are larger, Figure 4 (b).
The atomic size difference between base metal and alloying element atoms affect the lattice distortion. By increasing the size difference, the strain field around the solute atoms becomes stronger to resist against dislocation movement.

The created lattice strain filed around solute atoms raised the stress required to move the dislocations.

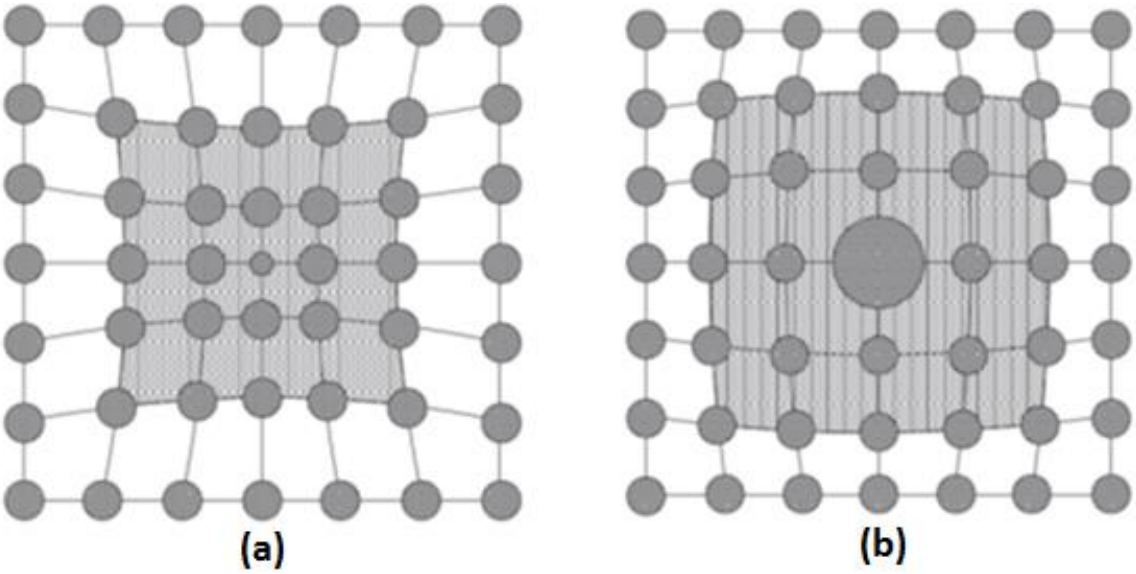

Figure 4 Subsitutional solid solution and high strained region in crystal structure [14]

The alloying elements with high solubility degree increase solute atom concentration. The solid solution strengthening mainly increases with higher solute atoms concentration, which solve in the matrix of the material [15].

3.3.2 *The precipitation hardening strengthening*

An effective mechanism, which improves mechanical properties of heat-treatable aluminium alloys, is precipitation- (or age-) hardening. This mechanism is associated with the formation of precipitates from a supersaturated solid solution in aluminium alloys. The basic requirement for precipitation hardening is that solid solubility limit should decrease with decreasing temperature. By decreasing the temperature, the solubility falls and aluminium matrix rejects the excess of atoms of the alloying elements. These atoms cluster into small precipitate particles. The

formation and distribution of such particles leads to strengthening of the material by obstruction of the motion of dislocations.

In order to have a dispersion of fine precipitate particle, the alloy is heat treated in three steps as follow [14]:

- **Solution treatment:**
  The goal of this stage is to dissolve the alloying elements and the formed precipitates in aluminium matrix. Solution treatment occurs at elevated temperatures above solvus line for a sufficient period of time and without melting the host metal to produce a homogenous single-phase solid solution.

- **Quenching:**
  Rapid cooling rate from solution heat treatment temperature usually to room temperature to obtain supersaturated solid solution in order to suppress immediate formation of second phase precipitate in the matrix. The alloy is a metastable supersaturated single-phase solid solution in this stage.

- **Aging:**
  In order to enhance the mechanical property of the heat treatable aluminium alloy, the supersaturated solid solution (SSSS) is reheated for convenient time to form finely dispersed precipitate particles.

The aging process can occur at room temperature, in this case, it is known as natural aging. This type of aging is a slow process and can take for several months. On the other hand, when the aging process is performed at elevated temperatures, it is called artificial aging.

The precipitation hardening process during aging time includes series of chemical and microstructural transformation. These transformations affect the mechanical properties of the alloys and may vary regarding to the type and concentration of alloying elements.

- Supersaturated solid solution:

By heating the material above solvus temperature, alloying elements dissolve in aluminium matrix. Then rapid quench results in formation of supersaturated solid solution as depicted in Figure 5.

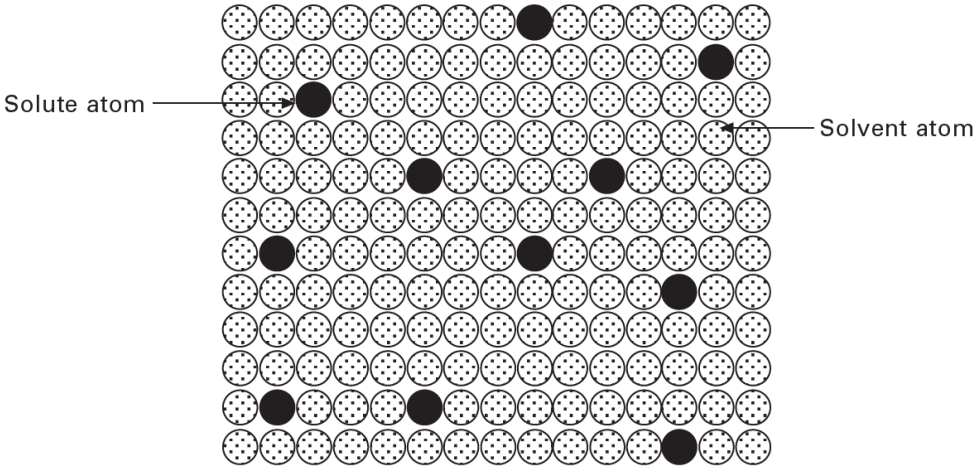

Figure 5 Super saturated solid solution condition

- Guinier–Preston (GP) zone:

With aging over the time, diffusional process activates and leads the solute atoms to position within the aluminium matrix in extremely fine-scaled solute enriched regions, which are known as GP1 zones.

By further aging to an intermediate temperature, ordered pattern of the solute atoms forms and develops, which are known as GP2 zones. Figure 6 shows the arrangement of GP1 and GP2 in lattice of the aluminium matrix.

The GP composition is determined by the dissolved alloying elements. The solute-rich zones are coherent with the parent matrix. GP zones are very small, typically one or two atom planes in thickness and several tens of atom planes in length. GP zones impose high strain in the surrounding lattice, which resist against dislocation slip.

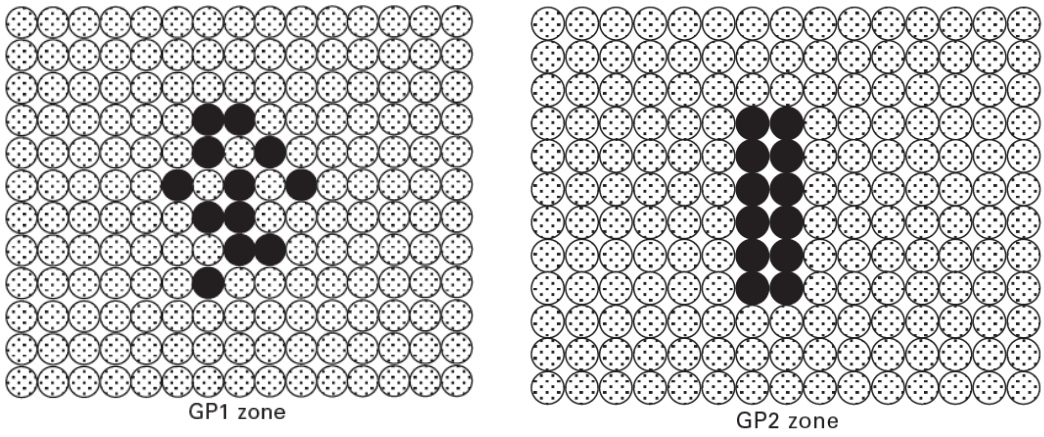

Figure 6 GP1 zone toGP2 during aging [14]

- Coherent precipitate:

With further aging, the GP zones transform into intermediate precipitates, which are much larger than the GP zone. Precipitates by continuing aging, experience different degree of coherency such as coherent or semi-coherent to the lattice plane.

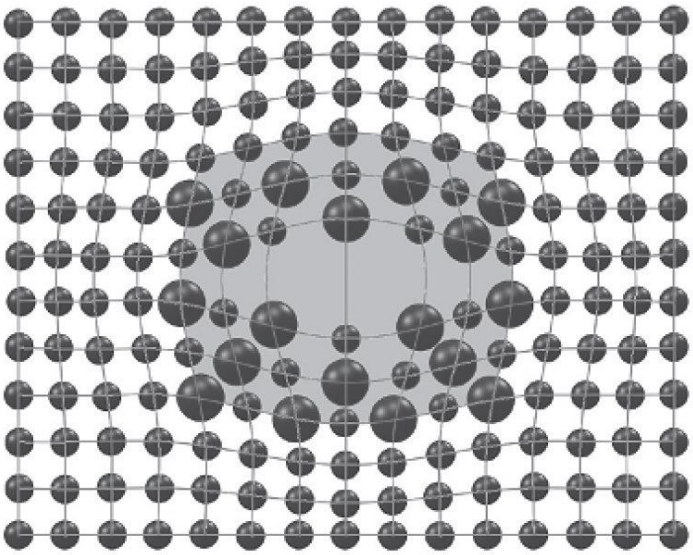

Figure 7 Coherent precipitates structure [14]

- Incoherent precipitates:

The intermediate precipitates transform eventually into equilibrium precipitate. The equilibrium phase is formed when the crystal structure does not change with more aging over the time. Distributed fine particles during coarsening change to larger precipitates. By coarsening the precipitates, the coherency between the formed particle and aluminium matrix will be lost, which leads to decrease in mechanical properties.

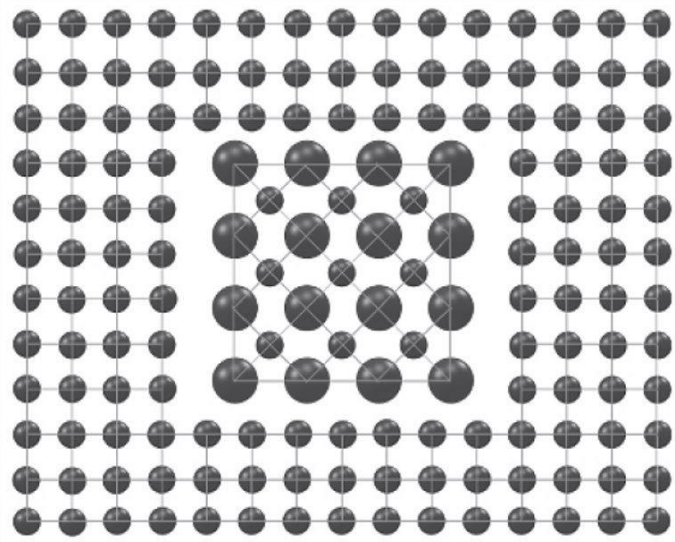

Figure 8 Incoherent precipitates structure [14]

Prolonged aging at too high temperature cause the large particle to grow still larger and the small fine particles disappear and replace with coarser precipitations. Higher aging temperature or aging time over the maximum gained strength reduce the material strength and is known as over-aging. The formation of incoherent equilibrium phases does not act as an effective obstruction to the dislocation slip, therefore leads to the softening of the material.

In the Figure 9, the effect of the thermal aging process on the strength of the material is depicted. The highest strength achieved where precipitates are coherent or semi-coherent to the aluminium matrix. The dashed line depicts the particle size during aging process.

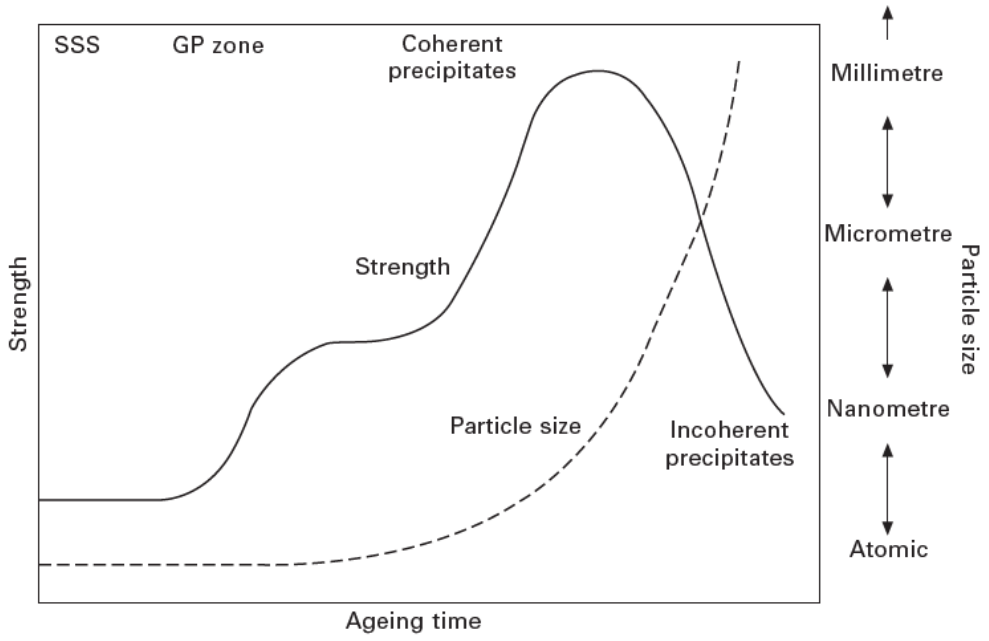

Figure 9 Strength and Particle size over the aging time [14]

The precipitation hardening is known as the most effective mechanism for heat treatable aluminium alloys. The formed precipitates while aging resist against dislocation movement, which increase the mechanical properties of age hardening aluminium alloys.

There are two ways to retard the dislocation slips. The dislocations are a type of lattice defects, which have great effects on mechanical properties. The plastic deformation occurs when the exerted force reaches the yield strength and cause the dislocation to move. When dislocations move, permanent deformation occurs by a process known as dislocation slip and result in plastic deformation. By applying below the yield stress, elastic deformation occurs, which results in interatomic bond stretching [14].

As a dislocation line reaches precipitates, it can either cut through the particle or bend and loop around and bypass them depends on the particle size and distance.

If the precipitates are very small e.g., coherent G.P. zones, dislocation can cut through the particle as shown in Figure 10. These fine precipitate particles provide a resistance to dislocation slip and cause improving the strength and the hardness of the alloy.

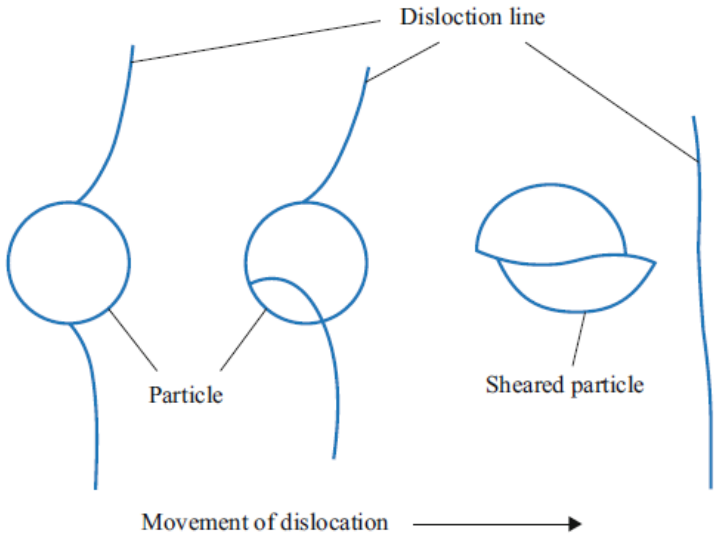

Figure 10 Dislocation cutting through the particle [15]

By further aging, the small precipitates grow larger e.g. incoherent precipitations. Coarsening the particles leads to reduction in number of particles and create more space between them. The dislocation line in this stage can only bend and loop around the particles. The strengthening effect is depicted in Figure 11 , which is known as Orowan mechanism [15].

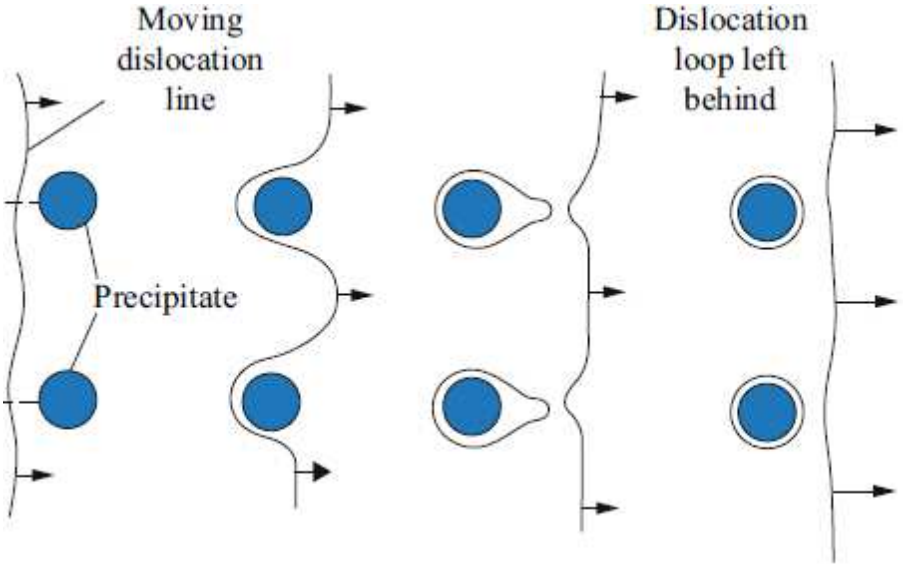

Figure 11 Dislocation bypassing widely spaced particles [15]

By increasing the aging time, the density of the precipitations decreases and precipitates space more widely. Thereby in this stage, the Orowan mechanism is less effective.

The strength of the alloy strongly dependent on the formed particle size and particles distance. As particle size and the space between the particles increase, lowering the overall strength is predictable. In Figure 12, deformable particles are the particles, which are sheared by dislocation and Non- deformable particle are the particles, which bypassed by dislocations.

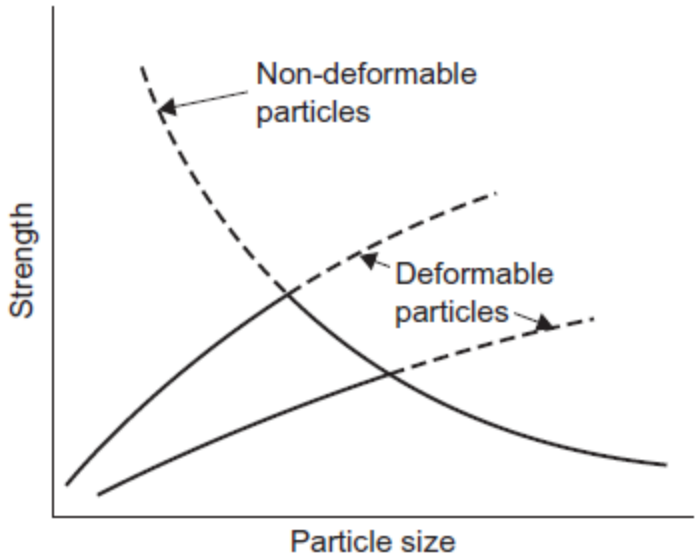

Figure 12 relationship between strength and particle size for particles sheared (deformable particles) and particles by passed (non-deformable particles) by dislocations

The maximum strength is reached for an average particle size, where two curves intersect.

3.3.3 *The related phases sequences to the produced alloy*

According to the alloy composition, during aging appear second phase precipitates, which are responsible for improvement of mechanical properties of the material.

The precipitation sequence during age hardening is a follow:

Supersaturated solid solution → Guinier-Preston (GP) zones → intermediate precipitates → equilibrium precipitates

The structure of intermediate phases, which are coherent or semi coherent to the lattice of aluminium matrix in Al-Zn-Mg-Cu system are [16]:

Phase	**Crystal structure**	**Lattice parameters**		
		a, nm	c, nm	β
M' (η')	Hexagonal	0.496	0.868	-
	Hexagonal	0.496	1.403	-
	Hexagonal	0.515- 0.523	0.848- 0.862	-
	Monoclinic	0.497	0.554	120 °
	Hexagonal	0.496	0.702	-
T'	Cubic	1.42- 1.44	-	-
	Hexagonal	1.39	2.75	-
S'	Orthorhombic	0.405	0.720	b=0.906 nm

Table 1 Crystal structure of metastable phases formed in commercial alloys of the Al-Cu-Mg-Zn system [16]

The most relevant equilibrium phases in 7xxx alloys Al-Zn-Mg-(Cu) system include [17] [10]:

- η-Phase (MgZn2) with Zn>Mg (high Zn: Mg ratio)
- T-phase [$(Al\text{-}Zn)_{49}Mg_{32}$ or $Mg_3Zn_3Al_2$] with higher addition of Mg, Zn: Mg <2.2
- S-phase (Al_2CuMg) by adding Cu as a major adding element in higher concentration than Mg, Cu>Mg

Based on the chemical composition of produced alloy Al- **3.5** Zn- **5** Mg- 0.3 Cu (wt %) with higher concentration of Mg in compare to Zn (Mg>Zn), the expected equilibrium phase is T-phase for the manufactured alloy. The structure of the T' phase is in Table 1 hexagonal with the given lattice parameter or intermediate phases T' or T" is body-centered cubic (bcc) with crystal structure close to T-phase T Al_{32} $(Mg, Zn)_{49}$] [16].

An overview of the possible precipitation sequence of T-phase in 7xxx alloy is given as below.

Early investigations show that precipitation process in the Al-Zn-Mg systems can be defined as [18] [19]:

SSSS $\rightarrow$ GP zones $\rightarrow$ intermediate phase η' ($MgZn_2$) $\rightarrow$ equilibrium phase η ($MgZn_2$) $\rightarrow$ equilibrium phase T [$(Al, Mg)_{48} Mg_{32}$]

The other studies reported [14] [20] :

SSSS $\rightarrow$ solute vacancy $\rightarrow$ GP zone $\rightarrow$ intermediate phase η' or T′$\rightarrow$ equilibrium phase η or T

SSSS $\rightarrow$ GP zones $\rightarrow$ Semi-coherent T′ [Al_{32} $(Mg, Zn)_{49}$] $\rightarrow$ Coherent T [Al_{32} $(Mg, Zn)_{49}$]

The recently precipitation sequence is stablished as [20] [21]:

SSSS$\rightarrow$ GPI zone$\rightarrow$ GPII zone or T′′ (intermediate phase)$\rightarrow$ intermediate phase T′$\rightarrow$ equilibrium phase T [Al_{32} $(Mg, Zn)_{49}$]

4 Experimental

In this part, the experimental procedure and equipment set-ups are explained.

Metallography were carried out to find the relative amount of porosities, which could have existed in the material by investigating the cross section of produced samples.

In order to characterize the hardness behavior of the new produced alloy, three different aging conditions were performed. The hardness measurements were carried out to obtain hardness evolution of the material during different aging processes where mechanical properties of the material change by precipitation of the second phase in the alloy.

Differential scanning Calorimetry (DSC) were performed to investigate the precipitation sequence of heat-treated alloy and by different heating rates.

Transmission Electron Microscopy (TEM) investigations were used to investigate the crystal structure of the formed phases during artificially aged conditions.

4.1 Material

The chemical compositions of the used material in this thesis are given in Table 2.

In the designed alloy the available amount of Mg is in much higher concentration than Zn in compare to the common 7xxx series alloys.

Element	Mg	Zn	Mn	Cu	Ti	Si	Fe	Cr	Al
Alloy	5	3.5	0.5	0.3	-	0.1	0.1	-	Balance

Table 2 Nominal chemical compositions (wt%) of the alloy

Wire Arc Additive Manufacturing (WAAM) method was applied by melting consumable wire electrode (GMAW) to produce the alloy component. In Figure 13 cross sections of the produced components are depicted.

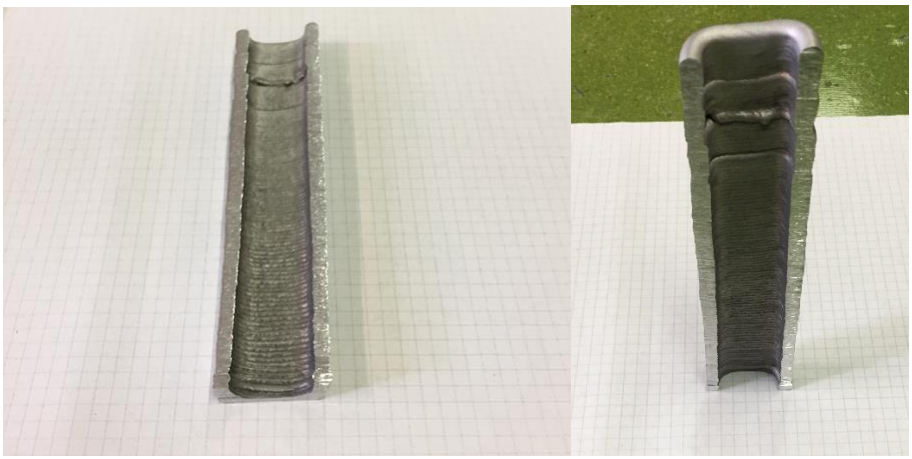

Figure 13 the produced part by Gas Metal Arc Welding (GMAW)

The production of the wire electrode, at the first stage, starts with melting of the chemical alloy composition. The melt then subject to heat treatment and followed by casting in cylindrical mold. The casted rods heated to temperatures between 440 to 460°C for extrusion process in order to reach the desired diameter [9].

4.2 Heat treatment

Heat treatment processes were done by Nabertherm RS80 tube quenched furnace, which was equipped with electronic temperature control and gas supply systems as shown in Figure 14. The sample suspends by a wire in the middle of the furnace tube.

Holding the alloy at the solution treatment temperature for a sufficient period of time. It is desirable to heat the alloy at the highest possible temperature without melting the aluminium to obtain supersaturated solid solution.

As the heat treatment process reaches the final process stage, the wire is cut immediately, and the sample will drop in the quench bath to quench the samples in water.

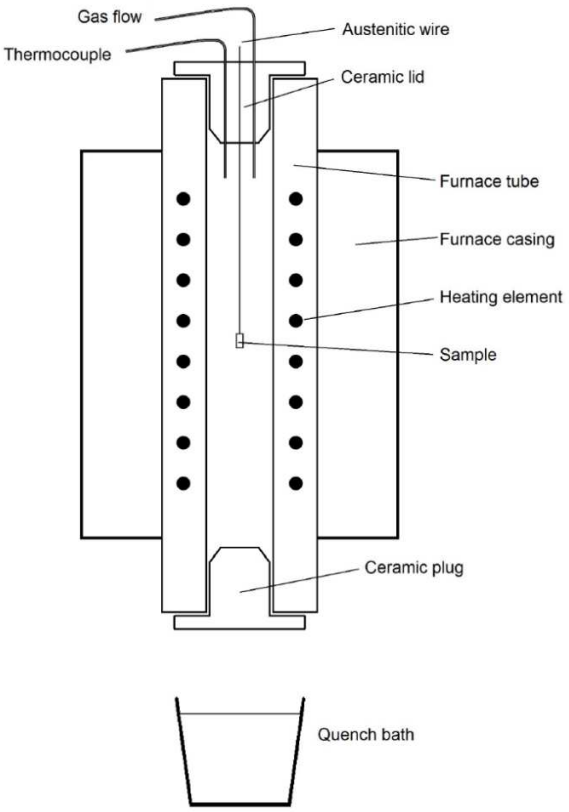

Figure 14 Schematic sketch of heat treatment quenching furnace

The samples were solution treated in vertical tube quench furnace as follows:

25-300°C for 15 min

300-400 °C for 15 min

400-500 °C for 15 min

At 500°C for 20 min

The samples experience different temperature levels during solution heat treatment process in furnace for 65 minutes to solve the alloying elements in the aluminium matrix. At the end of the heat process, the samples were quenched in water by cutting the wire, followed by aging for one hour in room temperature.

The heat treatable alloys, which has been given a solution treatment followed by quenching and natural aging (i.e. in air), are known as T4.

In Figure 15 the solution treatment curve for T4 condition is shown.

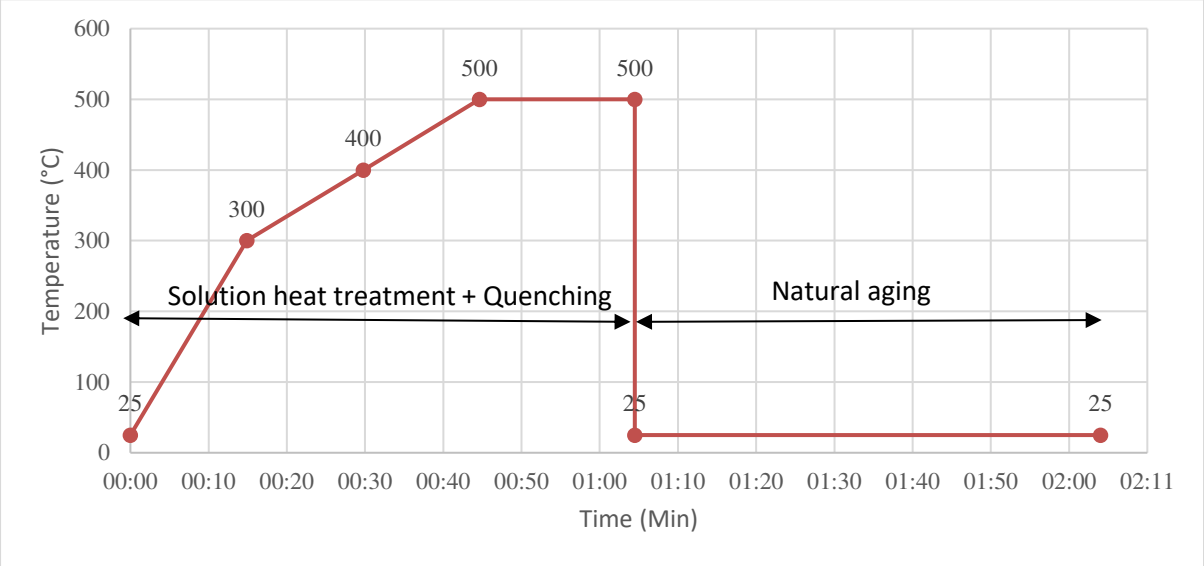

Figure 15 Solution treatment, T4 condition of the samples

4.3 Metallography

Metallography was done to examine the porosity of the manufactured alloy.

Preparation of the samples were in four steps:

Cutting and Mounting, Grinding, Polishing, Etching

The samples were cut by ACCUTOM 100 cutting machine and were then cold embedded. The samples were placed in a mounting cup and was filled with mixture of powder and hardening liquid of CEM3070. The sample orientation was selected perpendicular to the welding direction to investigate the welded surface under light microscope. The samples were grinded by abrasive papers of different grit sizes and were followed by polishing.

Etching was done in double step etching. The first step was done by lying the samples in etchant that was consist of 100ml distilled water and 2g NaOH for 1 minute at 40°C and then immediately in the other etchant, which was consisted of a mixture of 100 ml distilled water at 40°C and 4 g Potassium permanganate plus 1g NaOH. Samples in the second step was kept in the etchant for 20 seconds. After the etching process, samples were dried and were ready for investigation under the light microscope.

4.4 Differential Scanning Calorimetry (DSC) Measurements

Before Performing the DSC measurements, it was necessary to define the melting point of the alloy. Solution treatment temperature of samples should remain below the melting point of the material. It was necessary to find experimentally its melting temperature because there was no information about the melting point of the new designed alloy.

In order to find out the melting point of the alloy, DSC tests were performed by Netzsch (STA 449 F1 Jupiter) DSC/TG (Thermogravimetry) in rhodium furnace using Pt-Rh-crucibles with Al_2O_3 inlets. The selected heating rate was 20 K/min with holding time of 10min at 650 °C and the cooling rate of 50 K/min.

The measurement was executed and the related curve is depicted in the results chapter.

4.4.1 *Samples preparation*

In order to prepare the samples, the material was cut out in slices form with a thickness of ~3 mm using of ACCUTOM 100 cutting machine. The samples were stamped out from the slices in a disk form with a thickness of approximately 1 mm and diameter of 5 mm.

The punched samples were grinded with abrasive paper to reach the desired weight. The used material for reference sample was 99.9% pure aluminium. Both reference and sample were prepared similar in shape and weight.

For optimum resolution of the DSC measurements, the samples were prepared in a way to have a smooth surface as possible, which allow the samples to lie flat on the holders and obtain a good contact surface between the samples and the holders.

4.4.2 *Heat treatment sequence*

The T4 condition heat-treated samples, as explained in 4.2, were applied in DSC measurement.

Differential Scanning Calorimetry measurements were performed on TA Instruments Q20 with continuous heating rates of 2 and 5 and 10 (K/min) from 25°C to 500°C under pure nitrogen flow at a rate of 50 ml/min. During heating at some specific temperatures, phase transformations occur, which can be divided into endothermic and exothermic reactions. Endothermic process absorbs energy such as phase dissolution and melting. On the other hand, phase precipitation, recrystallization and oxidation are exothermic.

The DSC measurements heating process with different heating rates is shown in Figure 16.

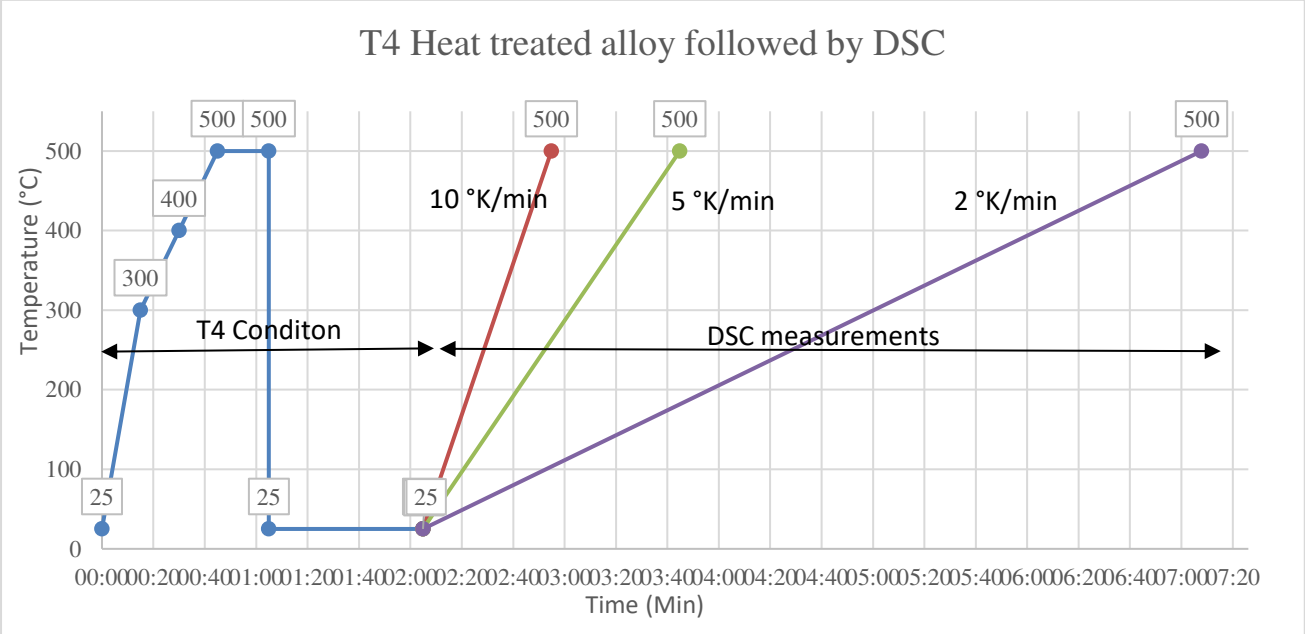

Figure 16 DSC for different heating rate

In order to obtain the DSC base line, the pure aluminium samples were placed in the both DSC holders, as sample and reference. For measuring the DSC signal of the alloy under the study, the second run was performed by substituting the high purity aluminium sample with alloy sample. The DSC curves for each heating rate were obtained by subtraction of the first run (base line) from the second run.

4.5 Hardness Measurements

For measuring the hardness, the samples of alloy were divided based on three different aging processes (single and two–step aging).

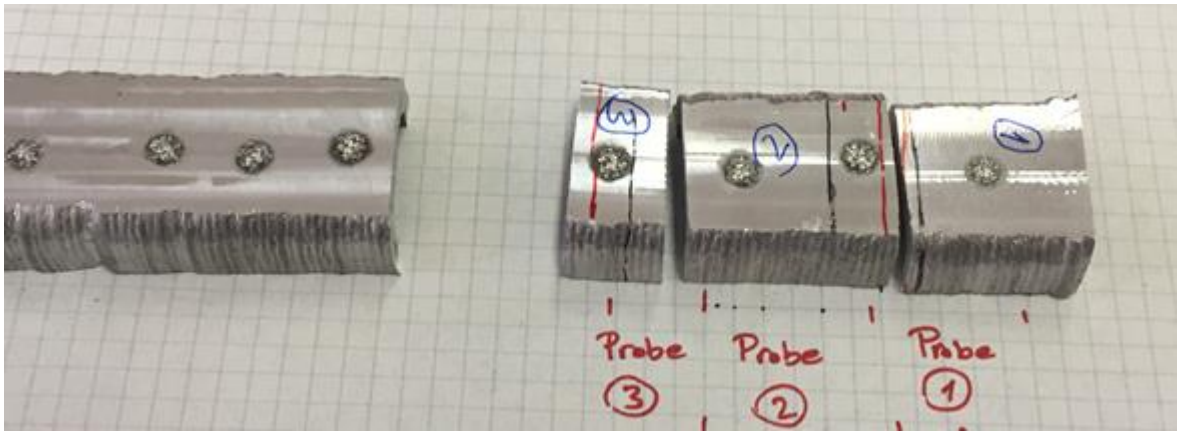

Figure 17 the three group of samples for Hardness measurements

The Brinell hardness tests were carried out with EMCO Test M1C-01machine during age hardening treatment in order to find the evolution of hardness during aging and preparing hardness curve evolution plots. The intender diameter was 1 mm with test load about 100 N and main load duration time of 10 second, with short designation as HBW 1/10. The hardness measurements were performed on the longitudinal surface cross section of the samples.

The sample surfaces were grinded by abrasive paper to maintain a flat surface in order to make visible indentation under the microscope. The hardness value for each measurement were obtained from three to five indentations on the samples. All the results were recorded by the computer in laboratory. For each hardness measurement during heat treatment cycle, the heat treatment process was interrupted for one hour.

4.5.1 *Sample Heat treatment*

The samples were solution treated in vertical tube quenching furnace, as before, and then divided into three groups and were heat treated in a MEMMERT UNE400 oven as per specified below aging process.

The solution treated T4 samples were aged as in the following:

- Sample (a) 90 °C for 24hours and then aged at 140°C for 622 hours
- Sample (b) 90°C for 500hours
- Sample (c) 140°C for 605 hours

4.6 TEM Investigation

The crystal structure of the formed precipitates in the samples during the aging were investigated using FEI TECNAI F20 Transmission Electron Microscopy (TEM), equipped with a field emission gun, an energy- dispersive X-ray (EDX) device and a high-angle annular dark field (HAADF) and scanning transmission electron microscope (STEM) detector. The operation was done with the voltage 200 kV. Complementary scanning-TEM (STEM) micrographs were obtained with a HAADF-detector for mass contrast. In STEM mode, energy dispersive x-ray spectroscopy (EDS) was used to estimate the local chemistry of the precipitates upon the characteristic x-ray emission.

The TEM samples were selected as follows:

- Sample (1) was aged at 90 °C for 24hours followed by aging at 140°C for 140 hours
- Sample (2) was aged 500 hours at 90°C
- Sample (3) was heat treated in T4 condition followed by heat treatment in DSC cell up to 275°C with heating rate of 10 K/min and immediately quenching in liquid nitrogen

4.6.1 *Sample preparation*

The required preparation steps are described below to reach the desired thickness of the samples for TEM investigations.

The thin slices from the heat-treated samples were grinded with Silicon Carbide abrasive paper. The samples were then sticked on a glass slide and grinded to a thickness of 100 μm, which was performed by 1200 grit abrasive paper for both sides of the samples. The samples were stamped out in a small disc form with ~3 mm diameter. The thickness of the sample in the middle was reduced to ~1μm by dimple grinder. Then Precision Ion Polishing System (PIPS) was performed which is equipped with ion guns using argon ions for sputtering on the surface of the sample. Ion beams were used for the atomic removal of the material. In the final thinning process, a hole was developed in the middle of the sample after several hours with the thickness of ~50-100 nm on the edge of the hole. The thin areas adjacent to the hole were used for TEM investigations.

5 Results

In this chapter, the results of the experimental parts are showed and summarised.

5.1 Metallography

The metallographic image from the produced alloy confirmed a quasi pore- and crack-free wall cross section with no sign of hot cracking tendency. Figure 18 shows metallography of the wall cross section along one welding layer.

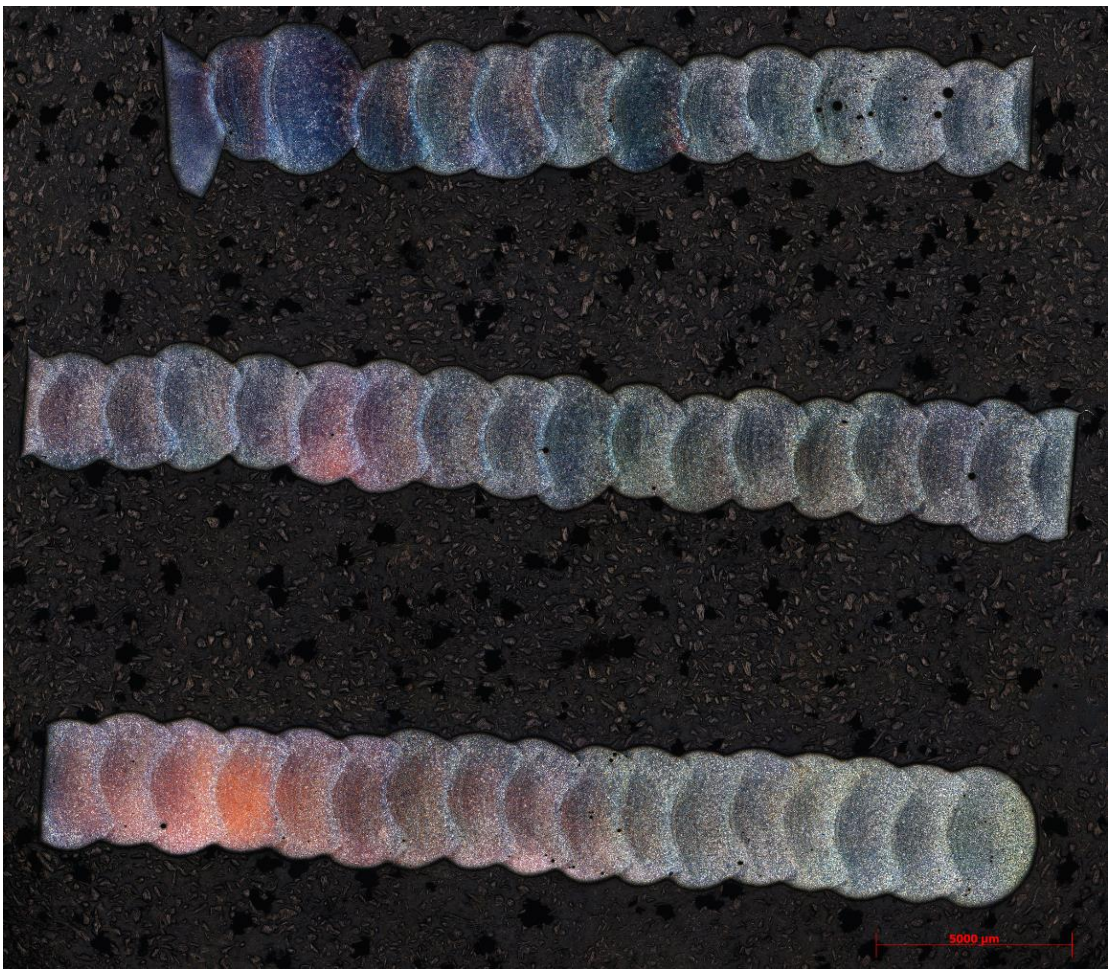

Figure 18 cross section of the etched sample

5.2 DSC Measurements

Begin of the melting of the material was found by using DSC and by recognition of strong endothermic peak. The found melting temperature then was used as upper limit of solid solution temperature. Any heat treatment or DSC were performed with some margin to the obtained melting temperature.

5.2.1 *Calculating onset melting points of the alloys*

The alloy was heated in thermal loops in the range between 300 to 650 ºC, which is depicted with red dashed line in Figure 19. In each loop two points with their slops were considered, one before beginning of the peak and the other one on the peak. For finding the slops, a linear behaviour of the curve from the point was assumed and the intersection of the slops were resulted in Onset point. The melting point of the alloy is the average of the onset melting points of each loop.

In the following figure, temperature and heat flow are shown in y-axis. According to the DSC results, the heat treatment temperature should be kept below 585°C for the alloy in order to prevent material melting.

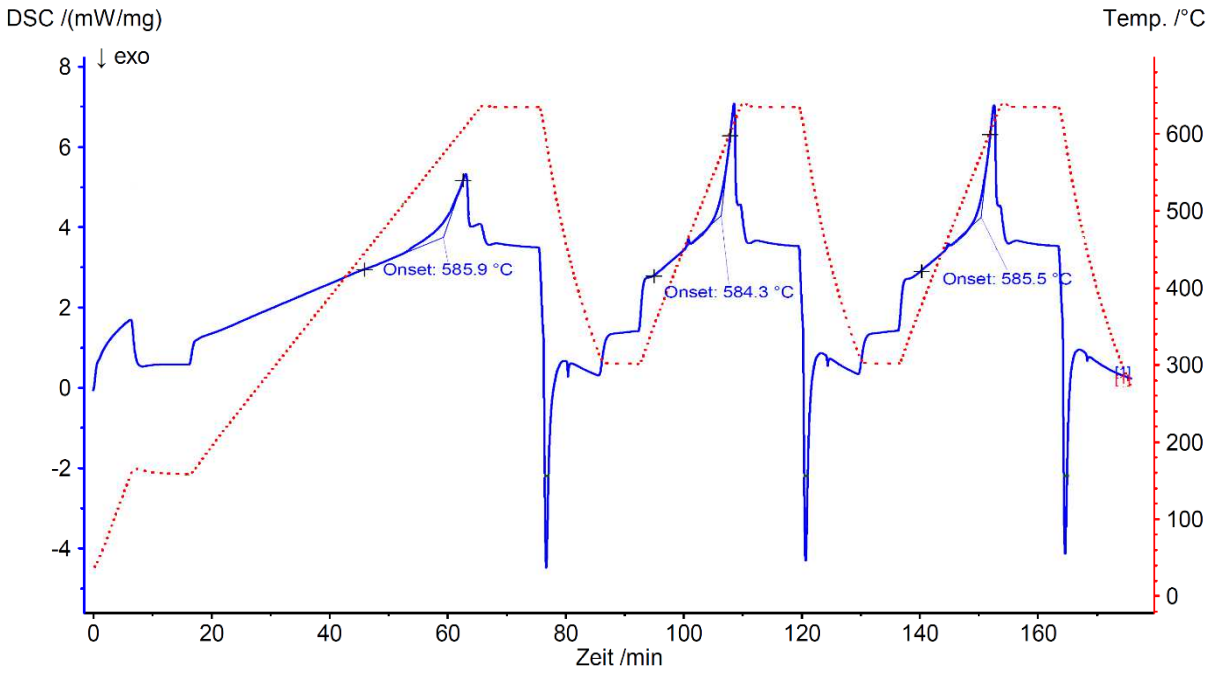

Figure 19 DSC for the Alloy

5.2.2 *DSC results for the alloy from T4 condition with different heating rates*

The samples were used in T4 condition for all DSC measurements related to thermokinetics investigation of the precipitations in the material. All the DSC runs began at 25°C to 500°C with the heating rates of 2 and 5 and 10 (K/min).

DSC measures the flow of energy as a function of time and temperature. With changing heating rate, the peaks will be moved or overlapped and they represent the kinetics and evolutions of the precipitates.

The difference in temperature in the sample and the reference material converted to a DSC signal in Watt [17].

With defining the weight of the samples, the DSC signal changes to W/g as below:

DSC signal (W/g) = Heat Capacity (J/(K g)) × Heating Rate (K/s)

In Figure 20 the DSC runs for the heat treated Al-3.5Zn-5Mg-0.3Cu alloy is shown, which exothermic reactions are in negative y-axis.

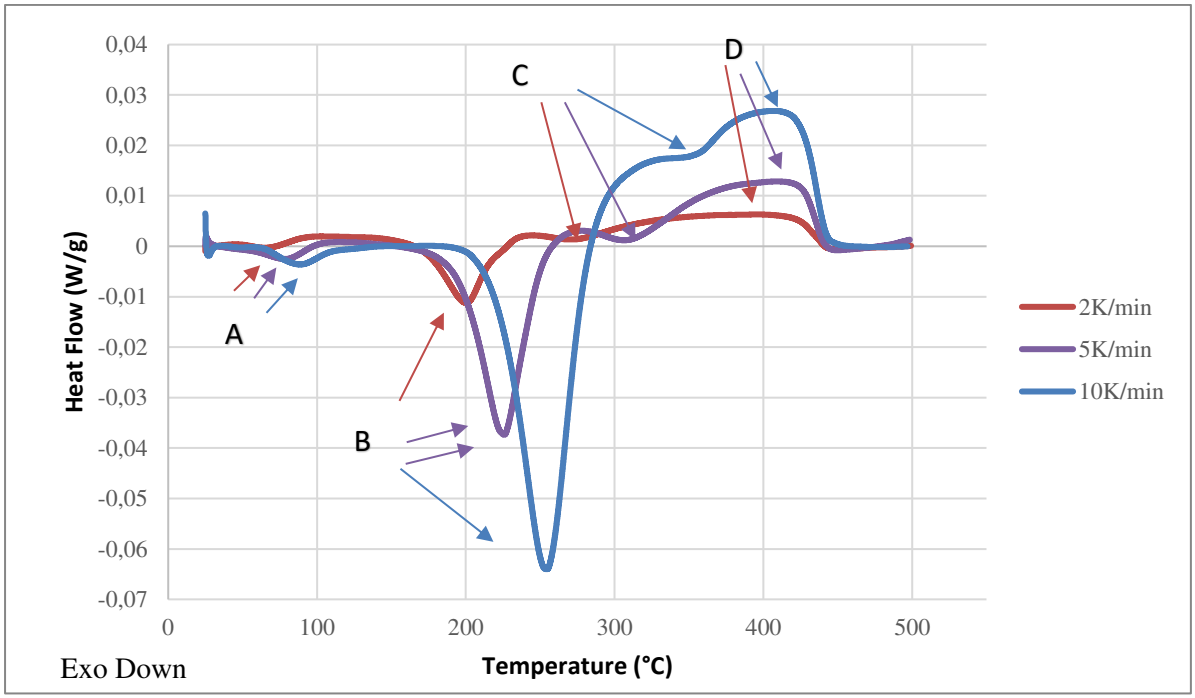

Figure 20 DSC runs for different heating rates

The DSC curves for each heating rate were obtained by subtraction of the base line from the second run. There are three exothermic and one endothermic peaks in DSC curves.

The peaks of A, B, C correspond to the precipitation reactions and peak D corresponds to the dissolution reaction.

5.3 Hardness Measurements

In Figure 21 evolution of the hardness of the material during different aging processes are given. Hardness curves plotted against the aging time for the three groups of aging processes. First group was aged at 90° C for 24 hours followed by aging at 140° C and for 622 hours. The Second and third group were aged at 90° C for 500 hours and 140° C for 605 hours, respectively.

The hardness value of the sample (a) was reached the peak hardness 160 HBW within 40 hours after pre-aging. For sample (b) with single aging of 90°C for 500 hours and sample (c) with 140°C for 605 hours, the peak hardness was 150 and 136 HBW respectively. Time to reach the peak hardness in sample (a) was decreased with artificial aging at 140°C, however in sample (b) and (c) the peak hardness value and time to reach the peak hardness were decreased with increasing the aging temperature.

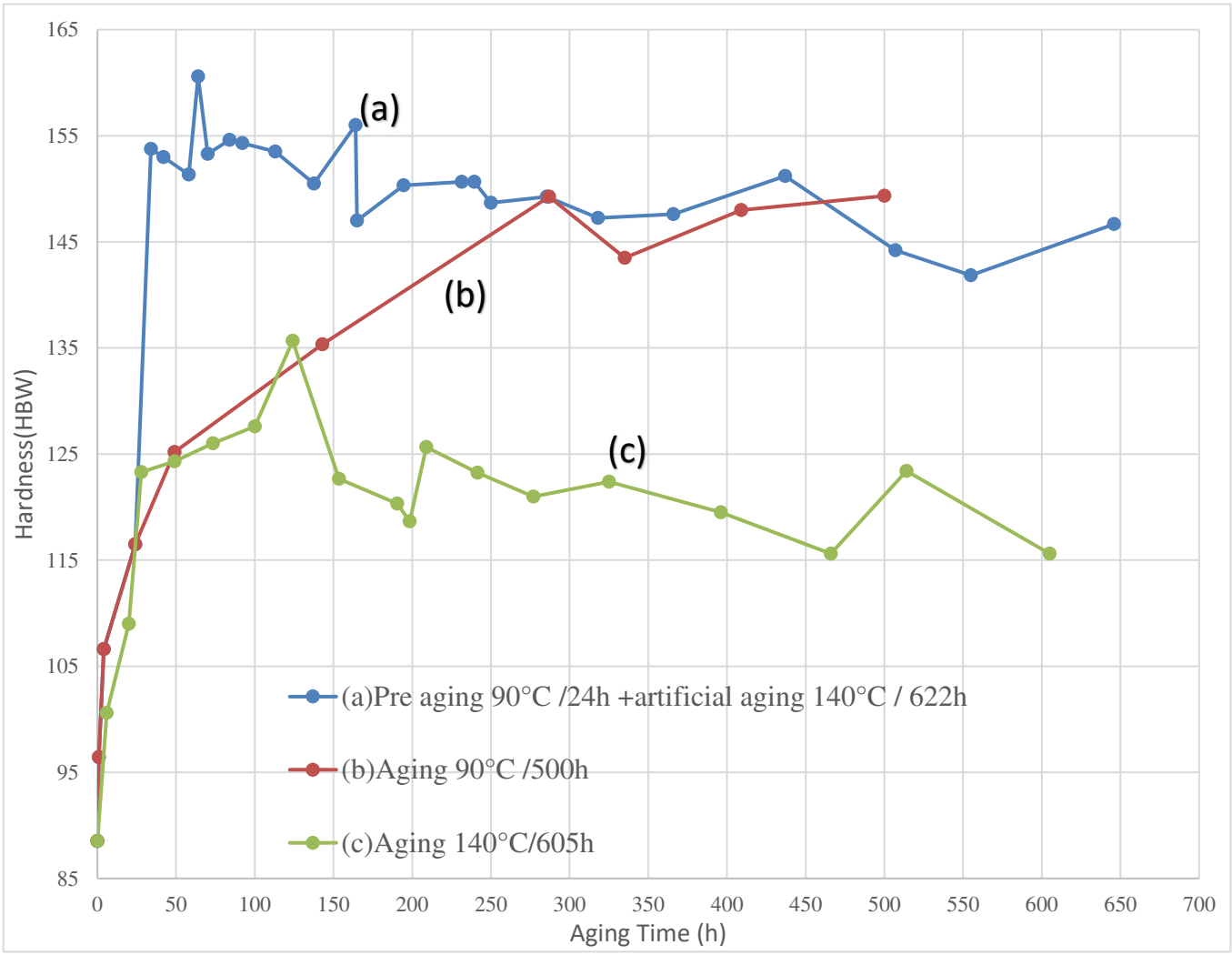

Figure 21 Hardness Curves for the alloy during artificial aging at (a) 90° C for 24 h and subsequently aged at 140°C for 646 h, (b) 90° C for 500 h and, (c) 140° C for 605 h

5.4 TEM Investigation

Three samples with three different heat treatment processes were chosen for TEM investigations. Sample (1) and sample (2), corresponding to sample (a) and (b) were selected from the artificially aged treatments at condition of peak hardness. These samples are specified as blue and red circles on the hardness curves in Figure 23.

Summary of heat treatment cycles for TEM samples are as below.

Sample 1: pre aging at 90 °C for 24 hours and aging at 140°C for 140 hours

Sample 2: was aged single step at 90°C for 500 hours.

Sample 3: was heated in DSC cell with a heating rate of 10 K/min to 275°C and interrupting the heat treatment by quenching the sample in liquid nitrogen.

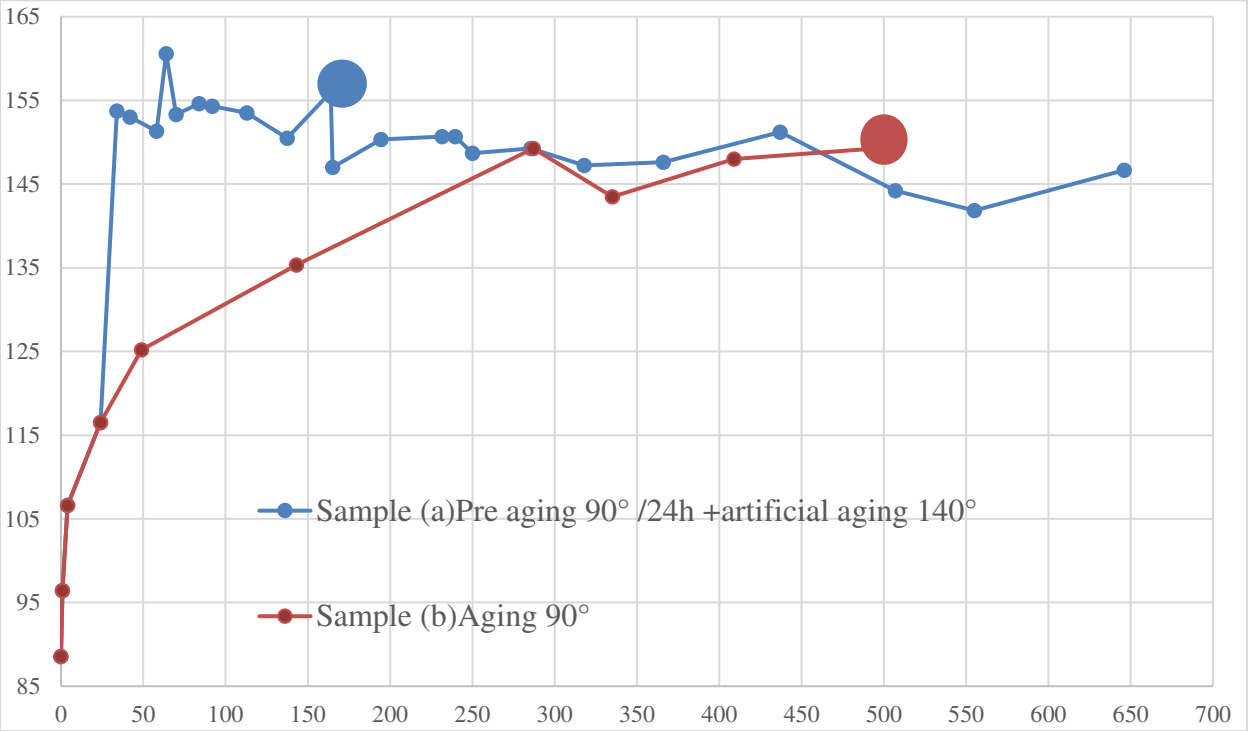

Figure 22 Sample (1) and (2)

The precipitates under TEM are categorized in three groups depends on the precipitates size in each sample. The large precipitates, which were found mostly on grain boundaries, medium precipitates and small one, which were found mostly in grains.

Different techniques as follow were used to obtain crystal structure image of the samples.

The high-angle annular dark-field (HAADF) detector in scanning transmission electron microscopy (STEM) mode was used to obtain mass contrast micrographs. In STEM mode, energy dispersive x-ray spectroscopy (EDS) was used to estimate the local chemistry upon the characteristic x-ray emission. TEM bright field (BF) were acquired mostly in the [110] zone axis of the matrix, in order to get overviews of the microstructure and distribution of precipitates.

5.4.1 *TEM investigation for sample (1)*

Sample (1) was investigated on TEM with pre-aging at 90 °C for 24hours and aging at 140°C for 140 hours. Overviews of the Scanning TEM HAADF and Bright field TEM of coarse the secondary phase are depicted in Figure 23.

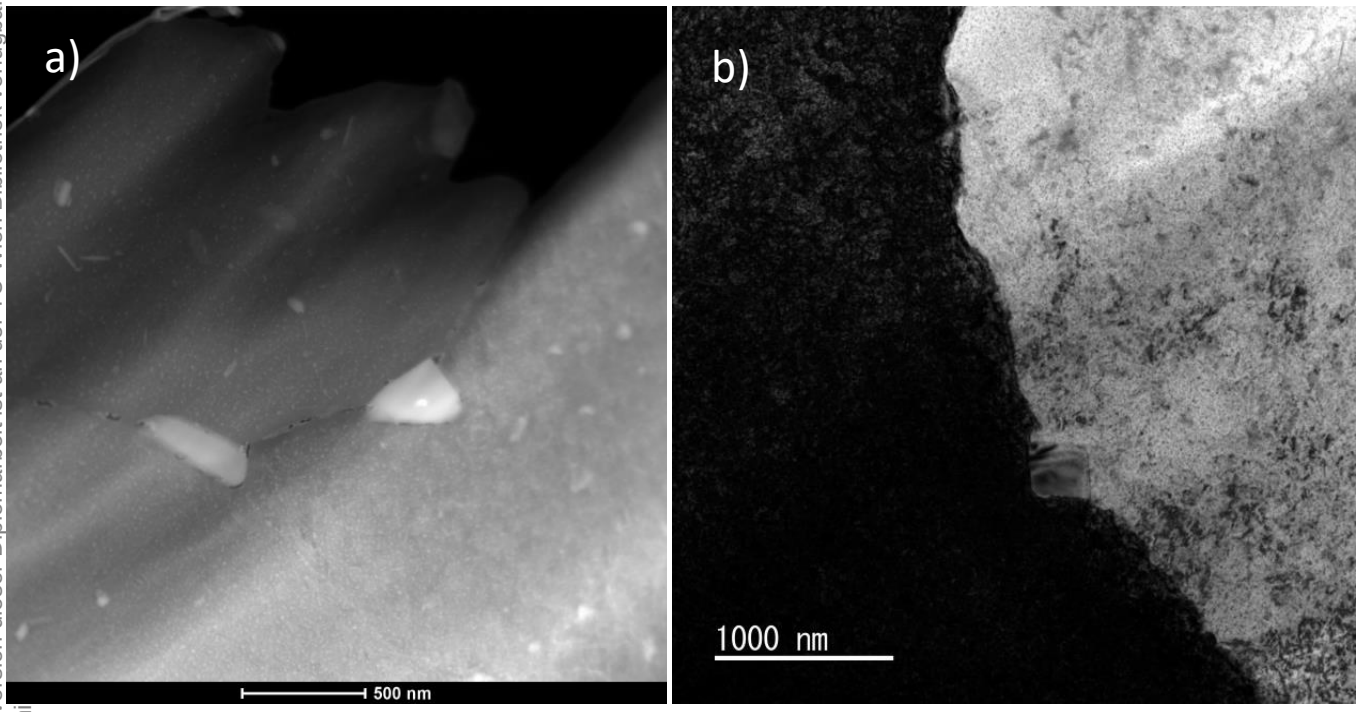

Figure 23 a) HAADF image and b)bright filed images of coarse secondary phase of sample 1

Two large precipitates in Figure 23 a) with the size of ~250 to 300 nm are visible. In TEM HAADF heavy atoms are observed brighter. In Figure 23 b), the grain boundary is easily recognizable which is located between two grains with different crystal orientations. The reason of different contrast in grains is due to different orientation to the zone axis. The crystal, which parallel oriented to a zone axis appears with dark contrast.

5.4.1.1 Large precipitates

Most of the large precipitates have been recognized on the grain boundaries. The EDX (energy dispersive x-ray spectroscopy) was used for analyzing of the local chemical compositions of the sample (1).The formed precipitates are showed in Figure 24.

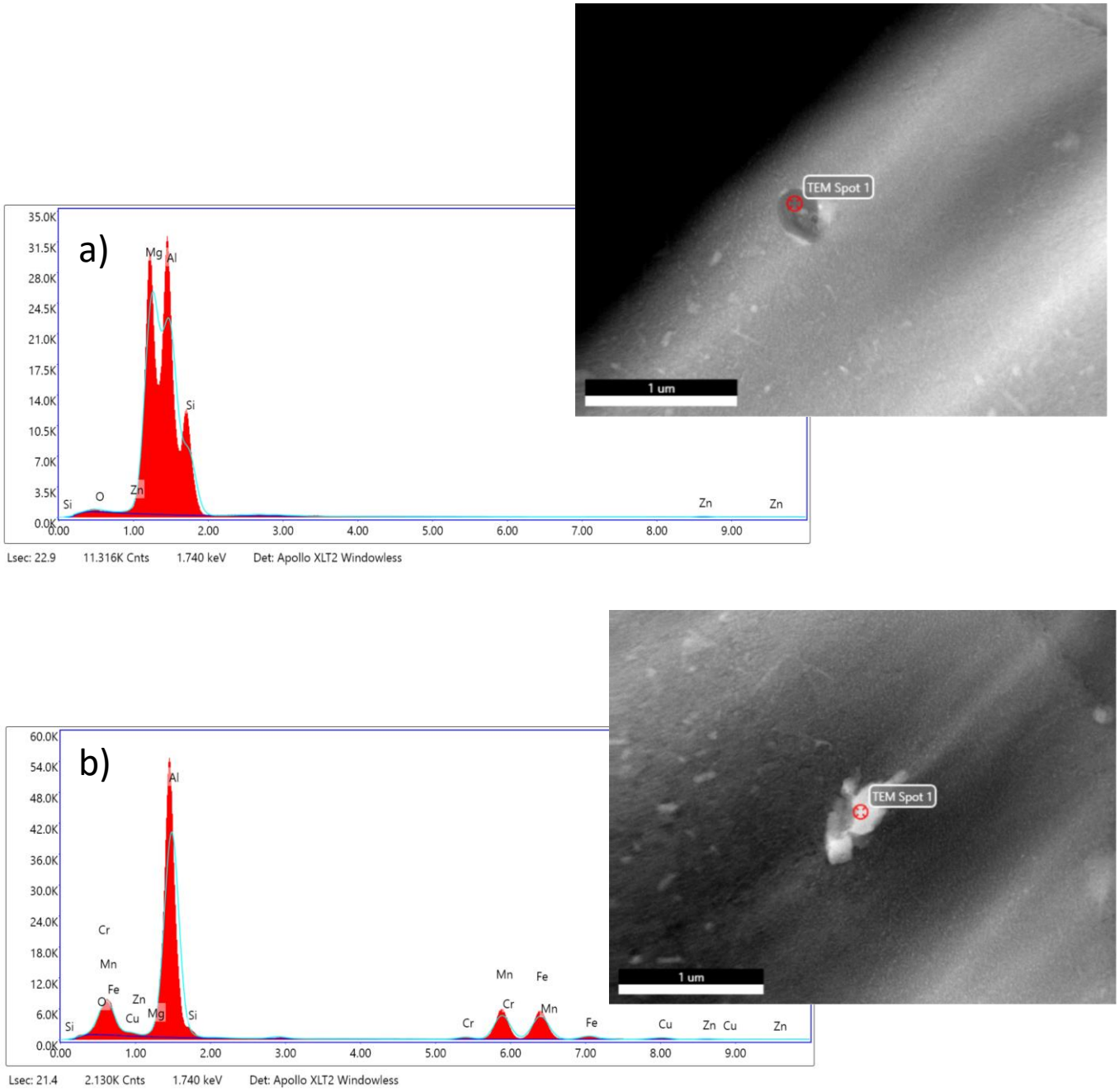

Figure 24 EDX analysis of STEM HAADF image show a) Mg_2Si and b) Al_6Mn

As can be seen in the above two figures, the formed precipitates are typically Mg_2Si and Al_6Mn in pointed spots.

5.4.1.2 Medium size precipitates

Most of the medium precipitates have been recognized in the grain boundaries. The bright field image below is an example of the medium size precipitations within the grain.

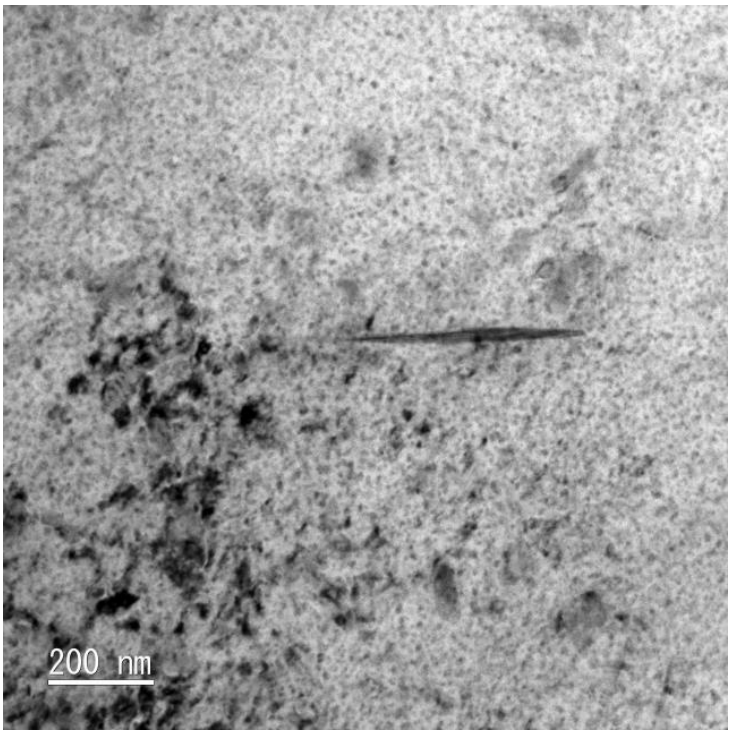

Figure 25 TEM bright field of medium size precipitates

The EDX image shows high amount of aluminium according to the heights of the peaks and then manganese rather than other alloying elements. Al_6Mn precipitates are inhomogeneously distributed within the grain in sample (1).

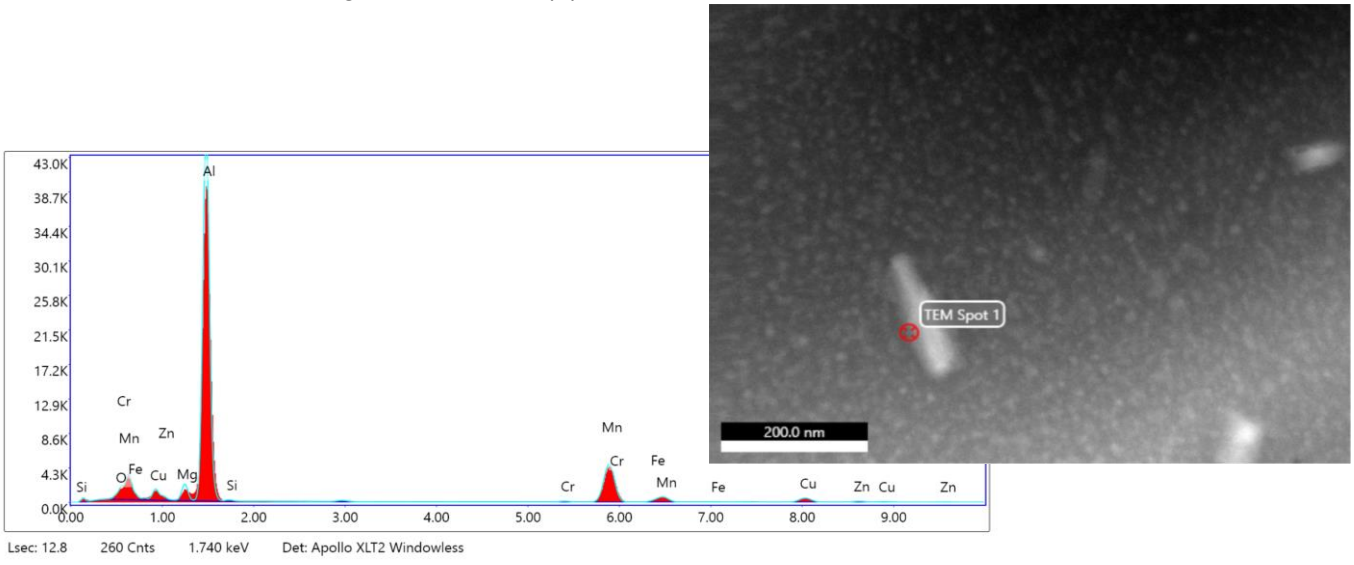

Figure 26 EDX analysis of STEM HAADF image showing Al_6Mn

5.4.1.3 Small size precipitates

The small precipitates have been recognized in the grain boundaries. High resolution TEM (HRTEM) images show coherent precipitates in grains for sample (1). As measured, the average diameter of the precipitates is about 10nm. The corresponding Fast Fourier transformation FFT was obtained to determine the crystal structure, the crystallographic orientation and the lattice parameter of the precipitates.

Based on Fast Fourier Transformation (FTT) pattern the indexing phase is T-phase. It is not easy to distinguish the different between T- and T'-phase. Some studies described T'-phase has the same crystal structure and the lattice parameter as T-phase [22] [16]. It should be noted that the indexing is not always unambiguous because different phases can produce similar diffraction patterns.

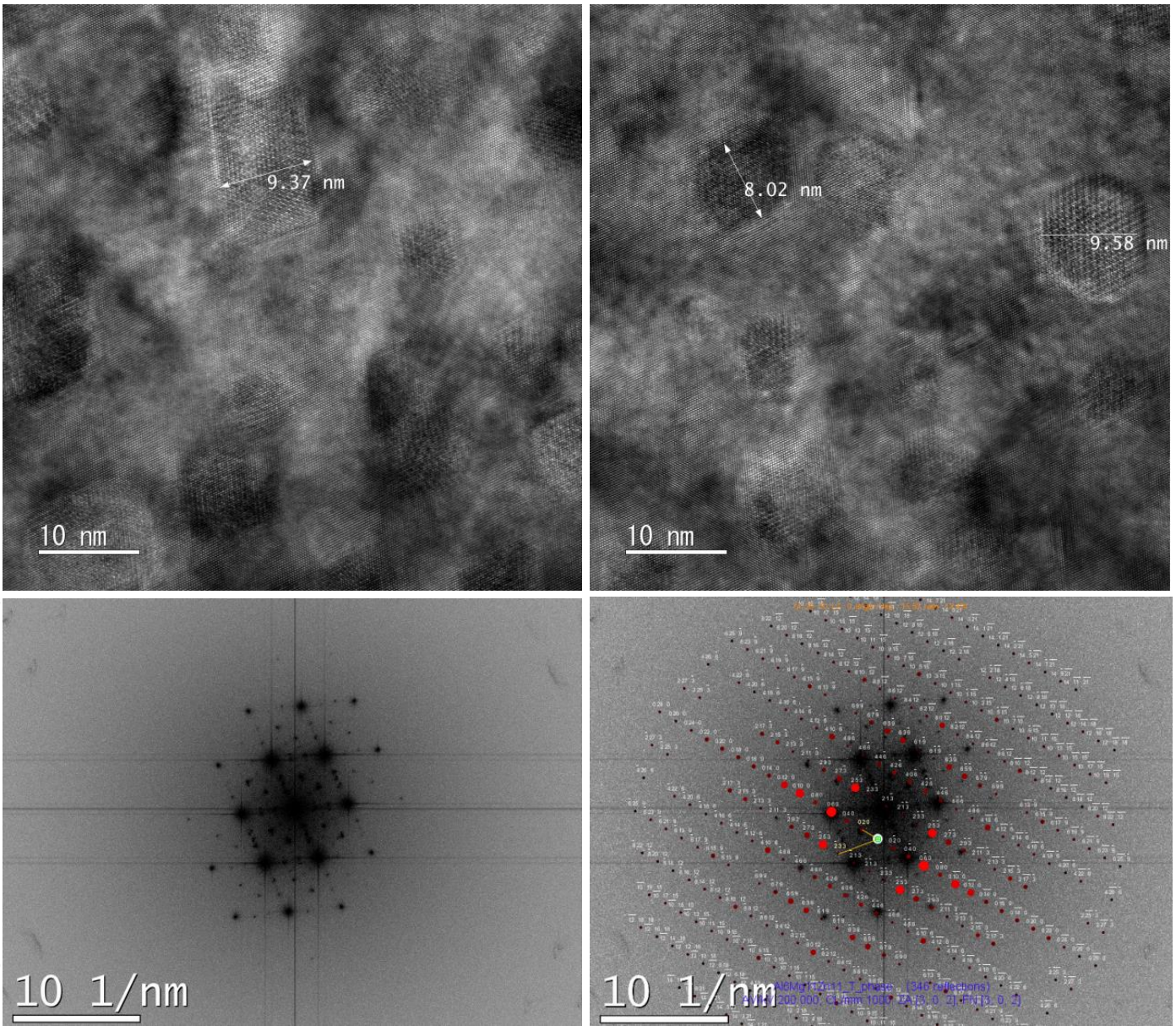

Figure 27 HRTEM image for sample 1 Fast Fourier Transformation(FFT) of sample 1 indexing T-Phase

5.4.2 *TEM investigation for sample (2)*

The Sample (2) was single step aged at 90°C for 500 hours. Overviews of the Scanning TEM HAADF and Bright field TEM of coarse secondary phases are depicted in Figure 28.

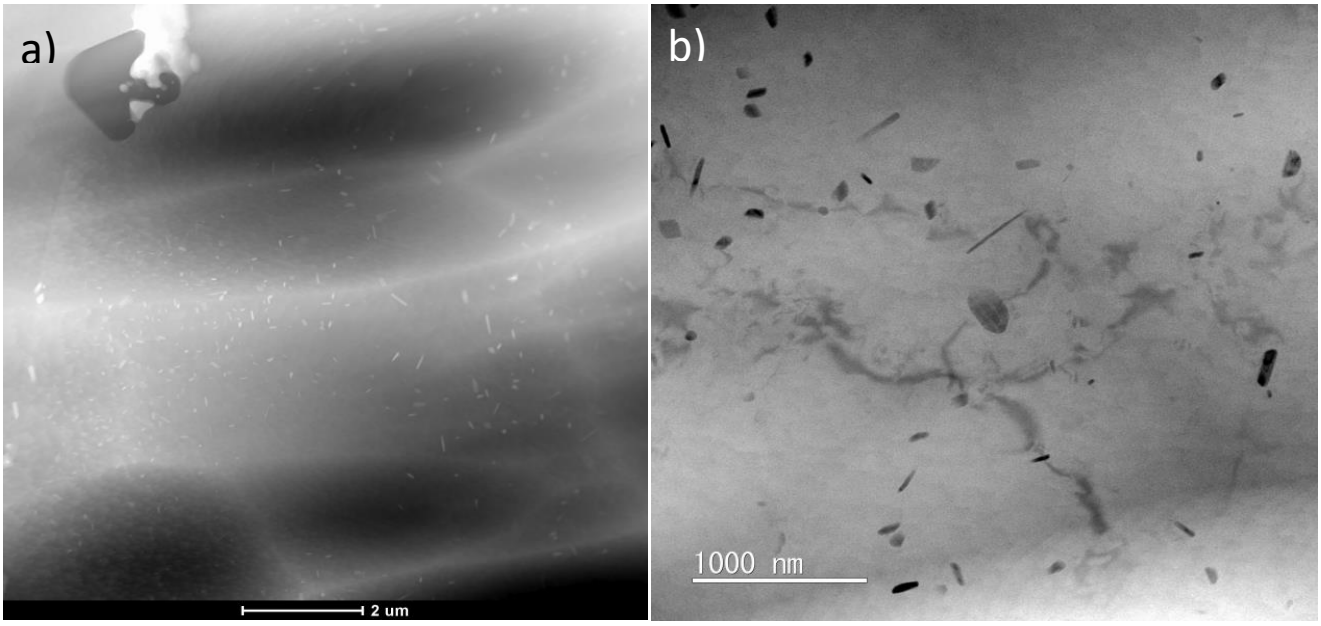

Figure 28 a) STEM HAADF image and b) bright filed images of coarse secondary phase in the sample 2

5.4.2.1 Large precipitates on grain boundaries

The EDX spectrum depicts the chemical composition of two spots on the precipitates. The detected precipitates according to the EDX analysis for chemical composition of sample (2) are depicted in Figure 29.

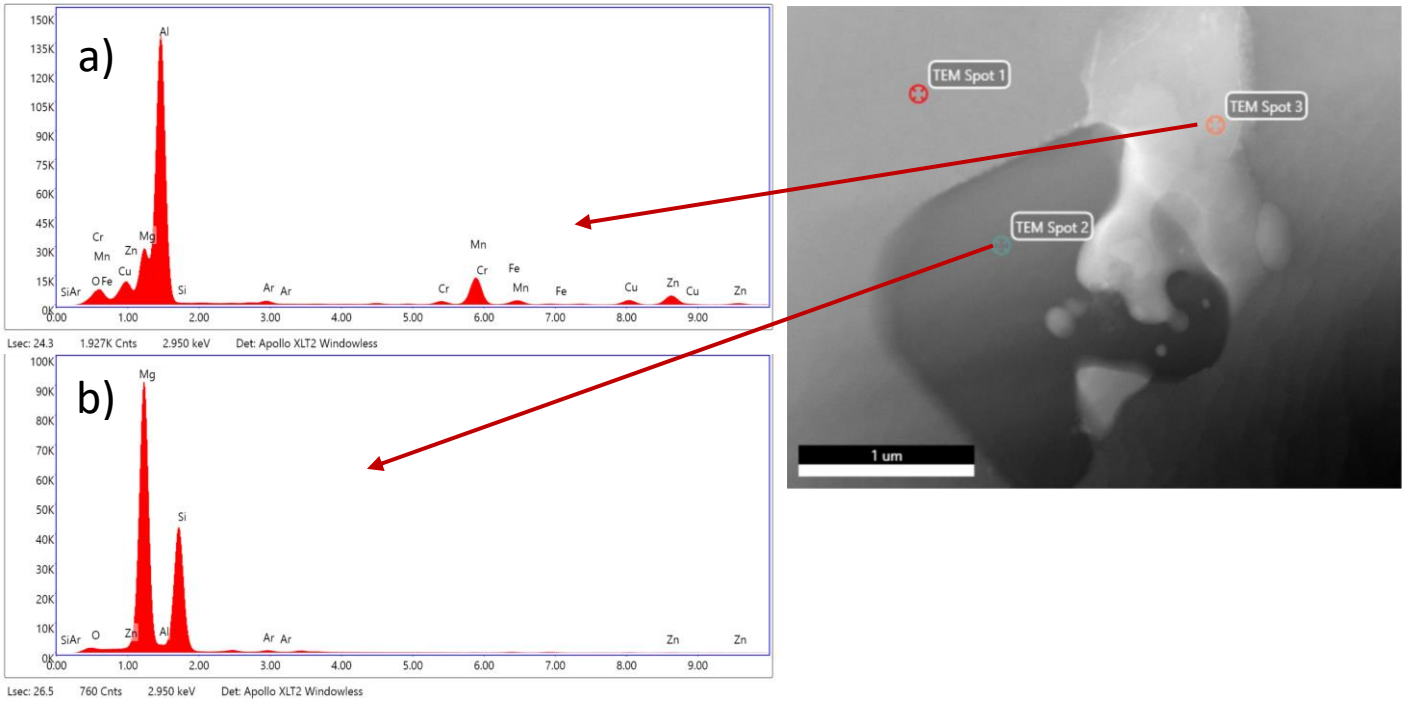

Figure 29 EDX analysis of STEM HAADF image show a) Al_6Mn and b) Mg_2Si

In Figure 30 bright field TEM shows the same grain boundary precipitates as in Figure 29. A large precipitate in Figure 30 with the size of ~2 µm is visible. Due to the contrast difference and different EDX spectrum in Figure 29 and Figure 30, we expect a compound of two different phases.

The crystallographic structure of the precipitates was obtained from the Selected Area Electron Diffraction (SAED) patterns. SAED results of the pointed areas are indexed in Figure 30 as a) Mg_2Si and b) Al_6Mn.

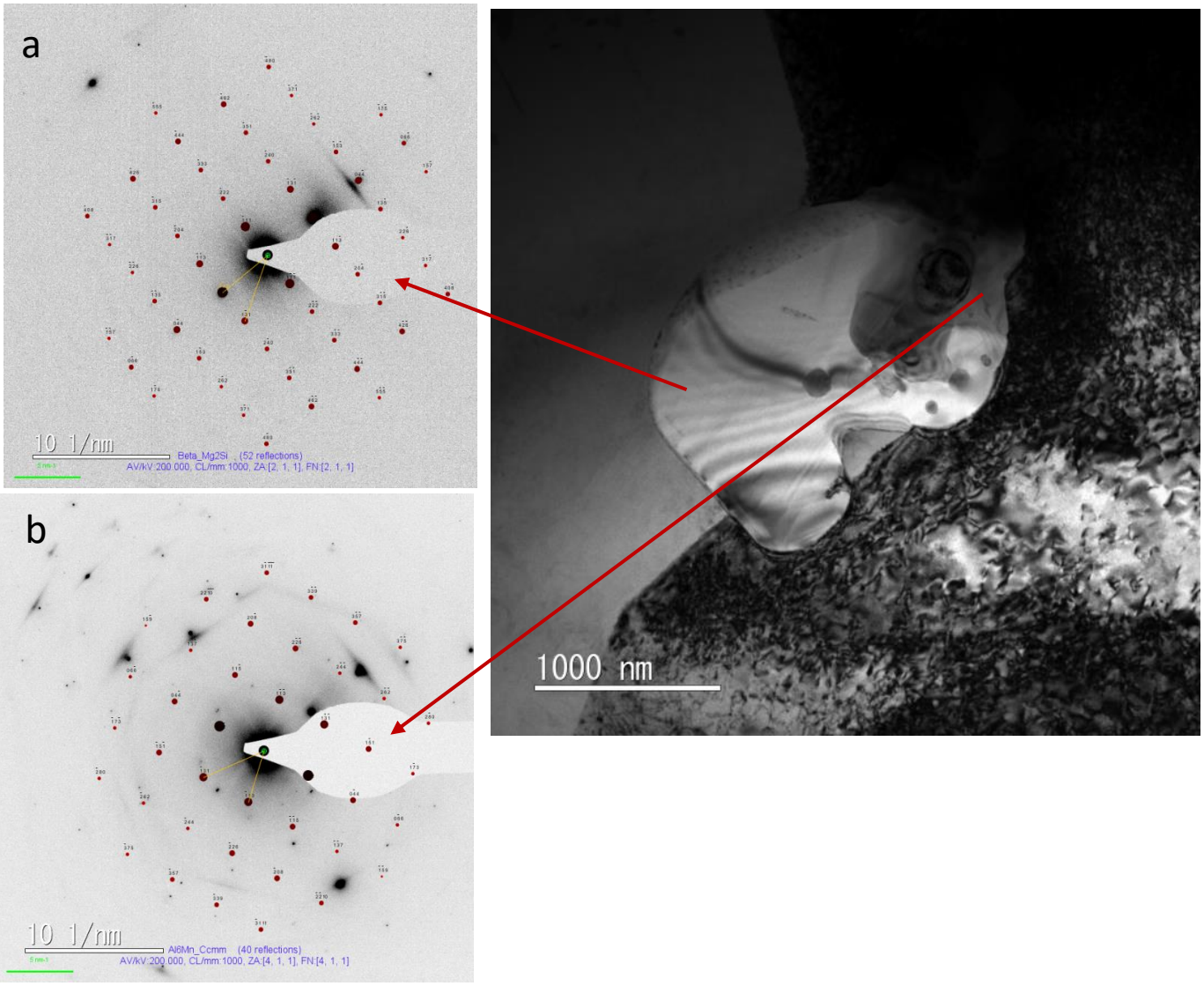

Figure 30 TEM bright filed with corresponding SAED pattern of pointed spots show a) Mg_2Si and b) Al_6Mn.

5.4.2.2 Medium size precipitates

Medium size precipitations in sample (2), which was aged for 500 hours at 90°C.STEM HAADF image in Figure 31 shows the very fine precipitation within the samples. EDX analysis corresponding to the STEM HAADF shows the chemical composition of $Al_{18}Mg_3Mn_2$ for pointed spot.

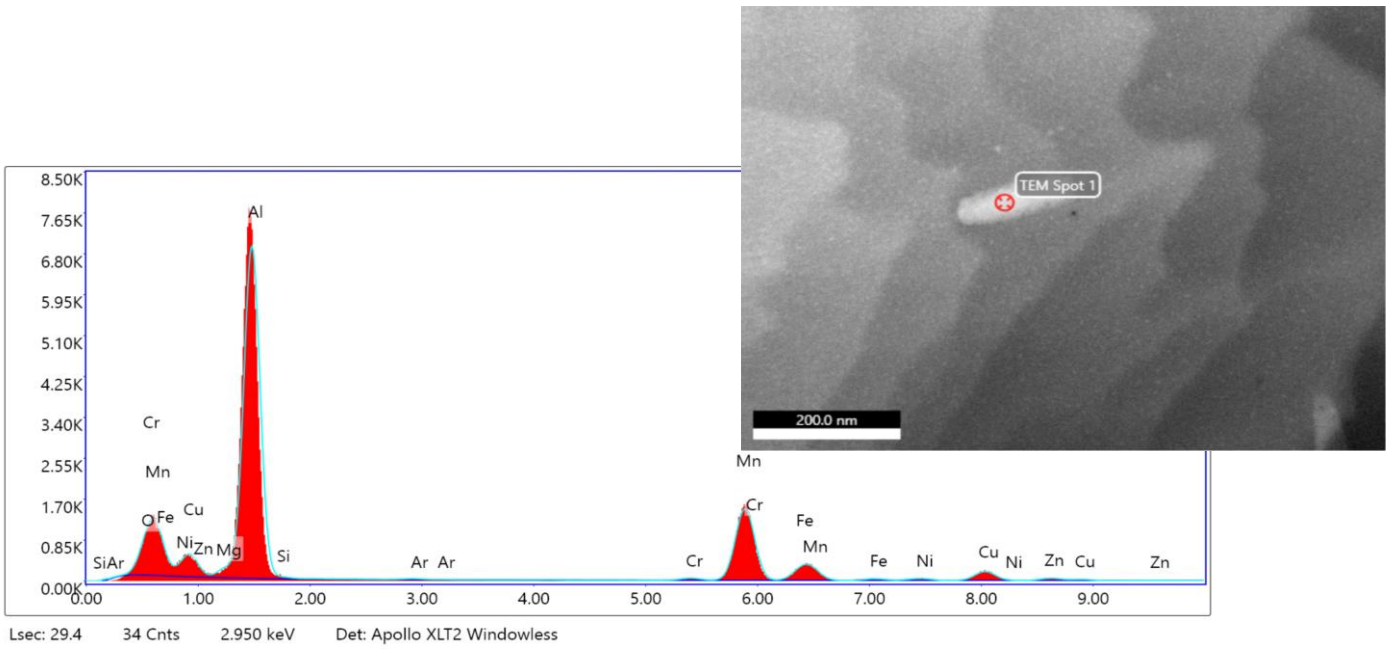

Figure 31 EDX analysis of STEM HAADF image showing $Al_{18}Mg_3Mn_2$

Selected Area Electron Diffraction SAED pattern were used to investigate the structure of the formed precipitation. According to the indexing of SAED the precipitate was identified as $Al_{18}Mg_3Mn_2$.

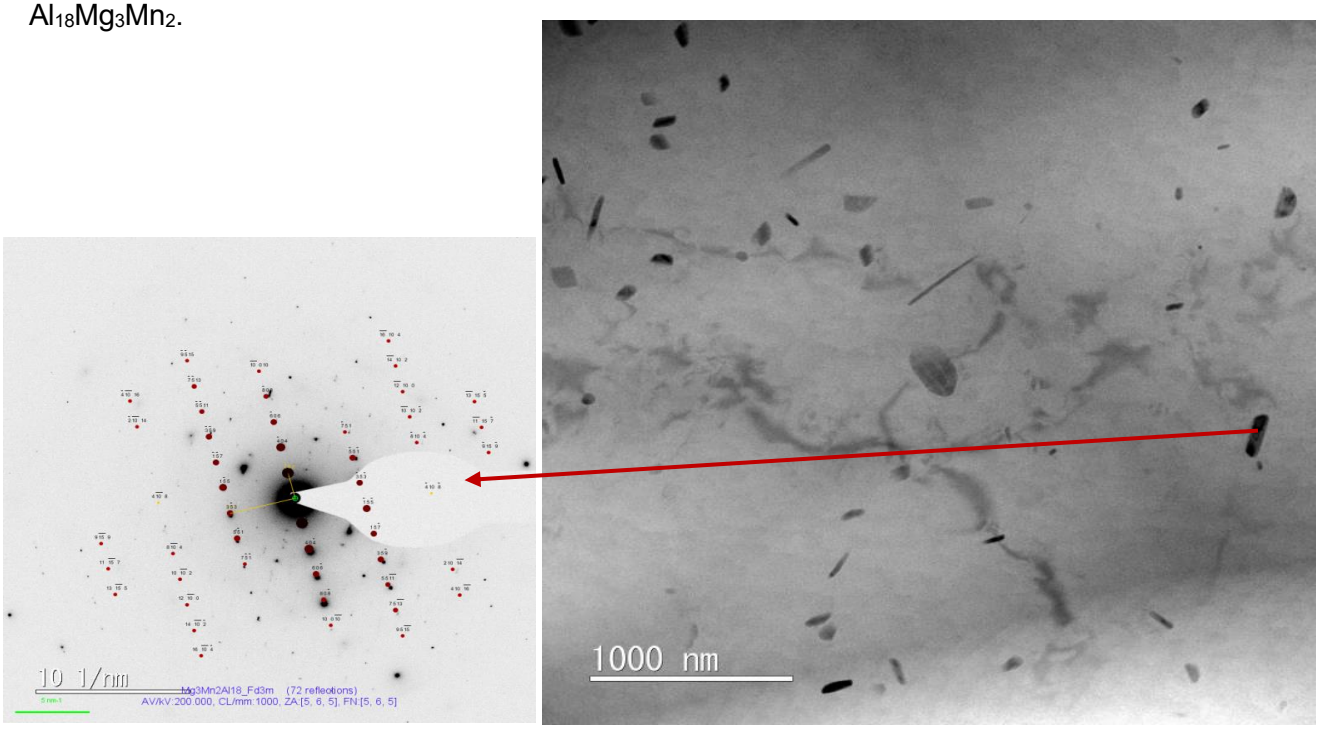

Figure 32 TEM bright filed with corresponding SAED pattern of pointed spot shows Al_{18} Mg_3Mn_2

5.4.2.3 Small size precipitates

TEM image in Figure 33 shows precipitates, which are distribute within the grains.

The mean diameter of the precipitations is about 5 nm. The precipitates could not be identified in terms of FFT indexing because of their small size.

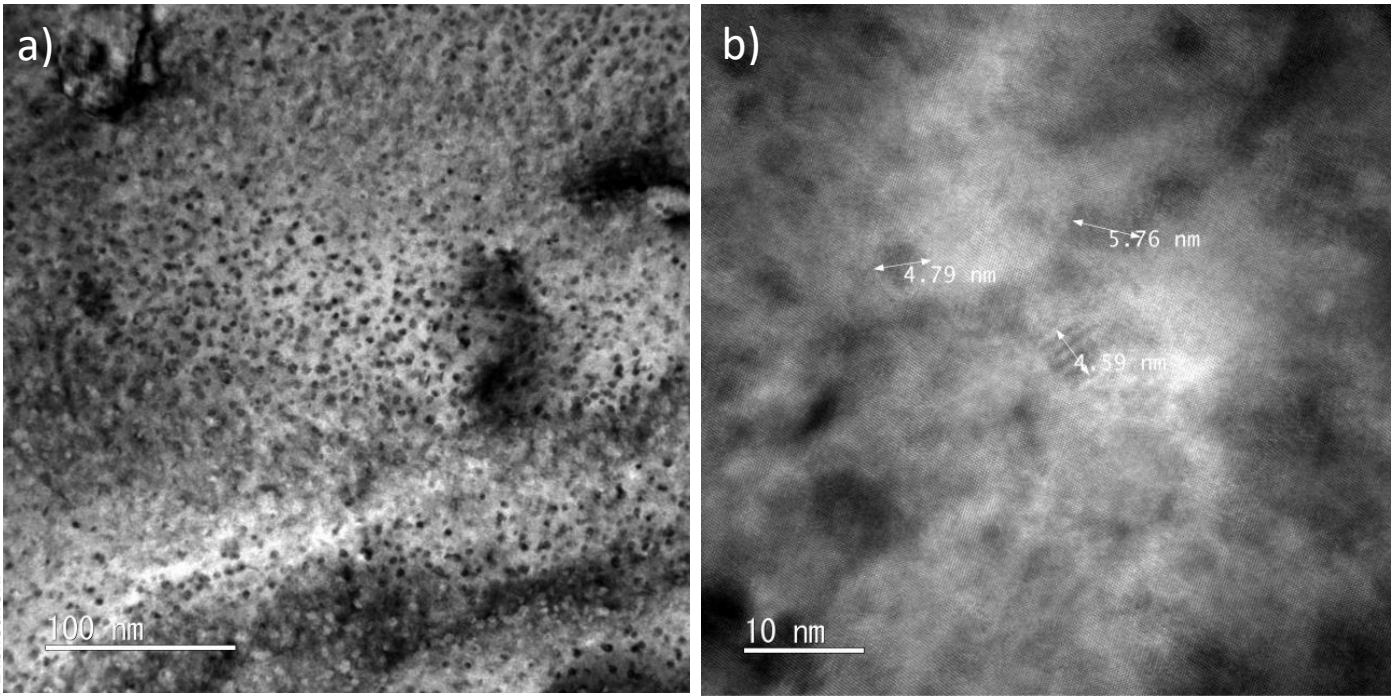

Figure 33 a) TEM bright field b) HRTEM image c)Fast Fourier Transformation(FFT) image of sample (2)

5.4.3 *TEM investigation for sample (3)*

Sample (3) was heat treated in DSC cell to 275°C and quenched quickly in liquid nitrogen. Beside the large precipitates, small precipitates are homogenousley distrbuted through the whole grain.

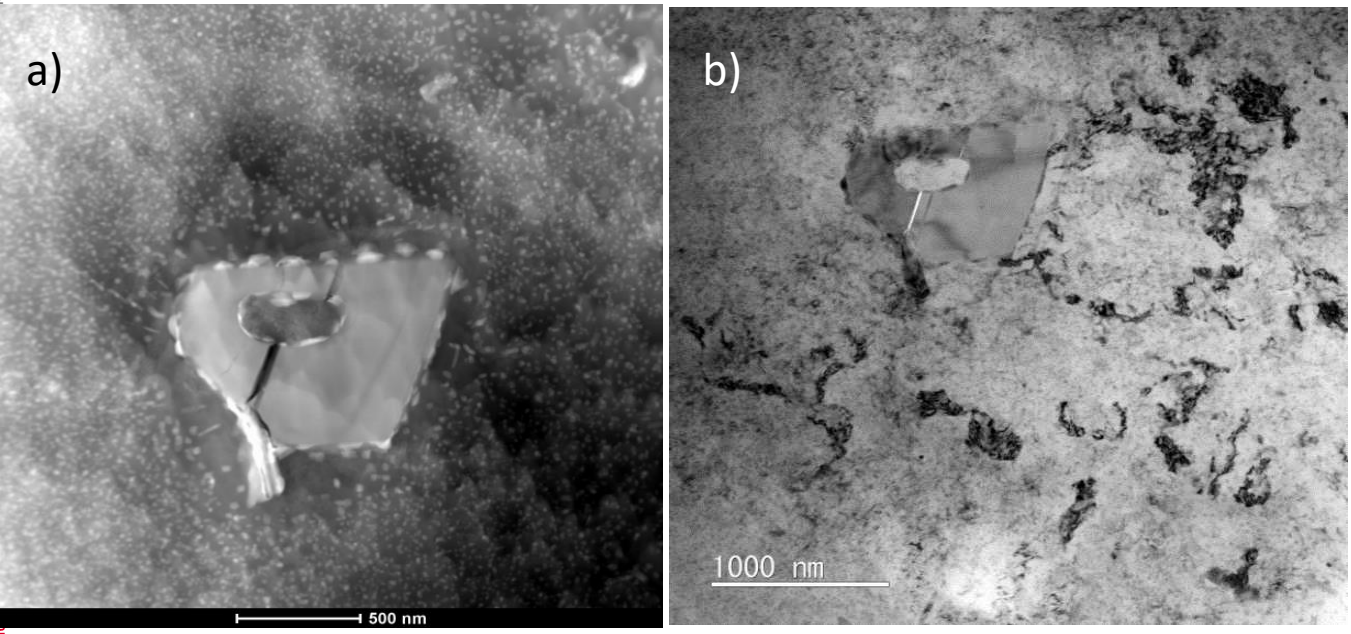

Figure 34 a)STEM HAADF image and b)bright filed images of coarse secondary phase of sample (3)

5.4.3.1 Large precipitates

In Figure 35 STEM HAADF and corresponding EDX spectrum are shown.EDX analysis was used in to estimate the chemical composition of the large formed intermediate precipitation.

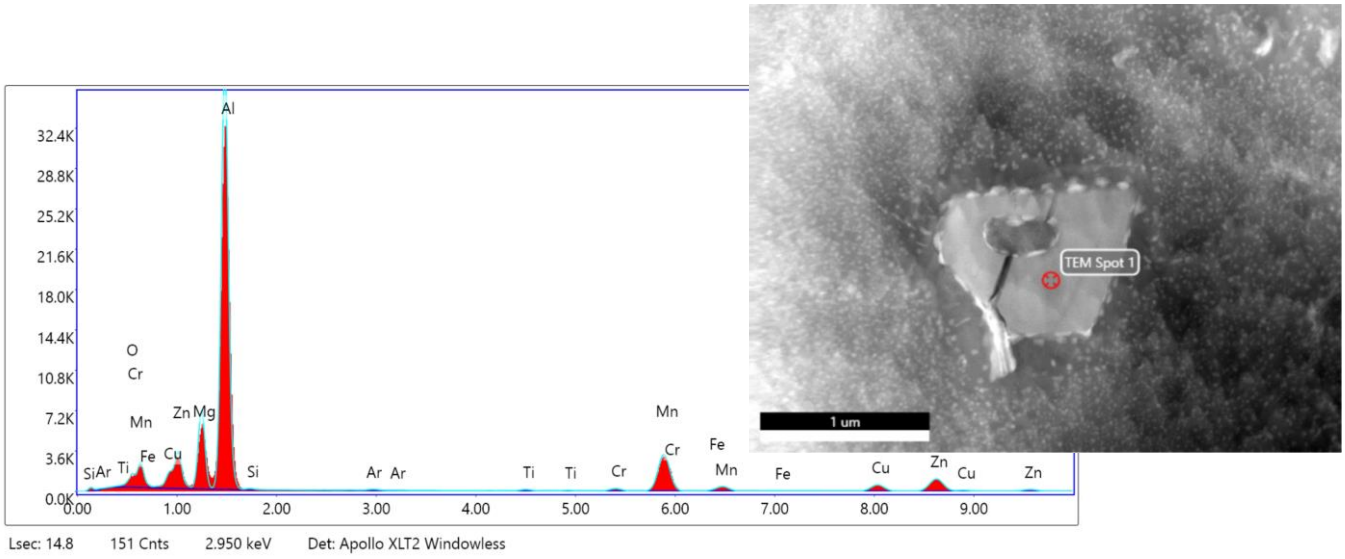

Figure 35 EDX analysis of STEM HAADF image showing Al_6Mn

The precipitation size is ~ 1µm.SAED pattern was used to identify the crystal structure of the precipitation. According to the SAED pattern the observed precipitate is Al_6Mn, which was detected also in, is sample 1 and 2.TEM Bright filed image and corresponding SAED pattern are showed in Figure 36.

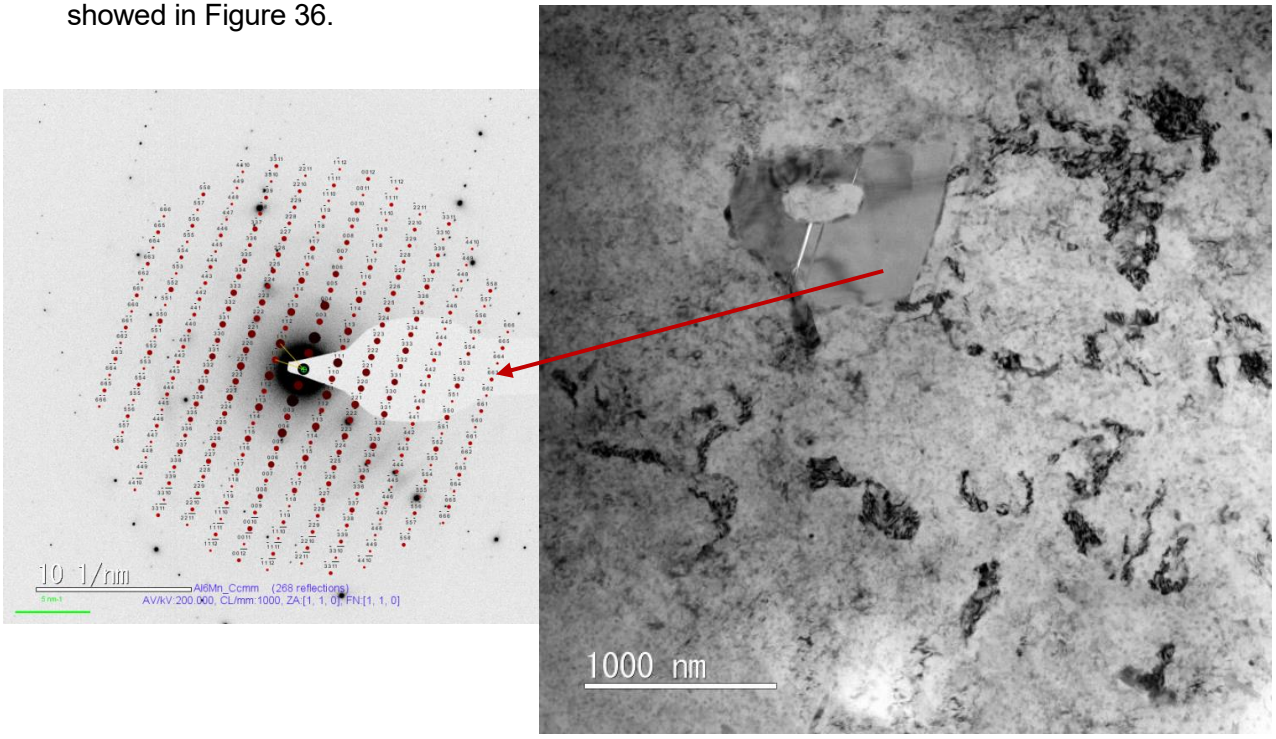

Figure 36 TEM bright filed with corresponding SAED pattern of pointed area shows Al_6Mn

5.4.3.2 *Medium size precipitates*

The found precipitate was analysed by EDX to estimate the local chemical composition in Figure 37. SAED pattern also was used to investigate the crystal structure of the precipitate.

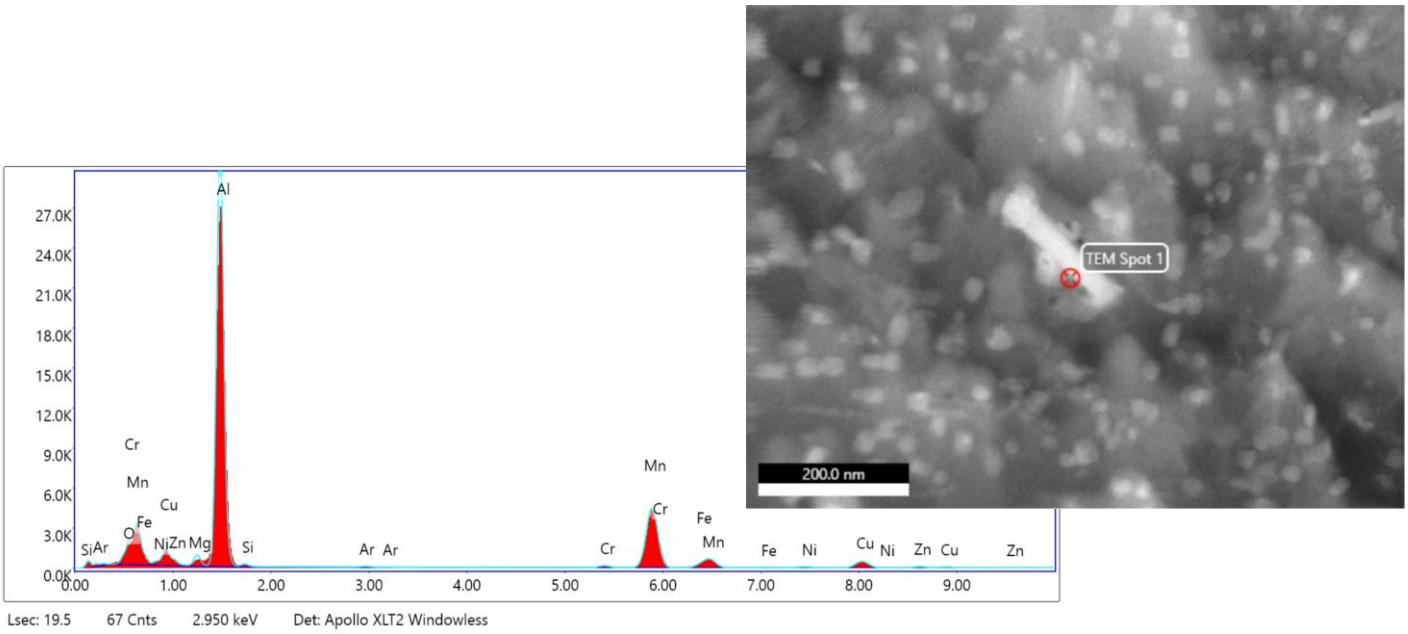

Figure 37 EDX analysis of STEM HAADF image showing Al_6Mn

According to the indexing of SAED the precipitate was identified as Al_6Mn.

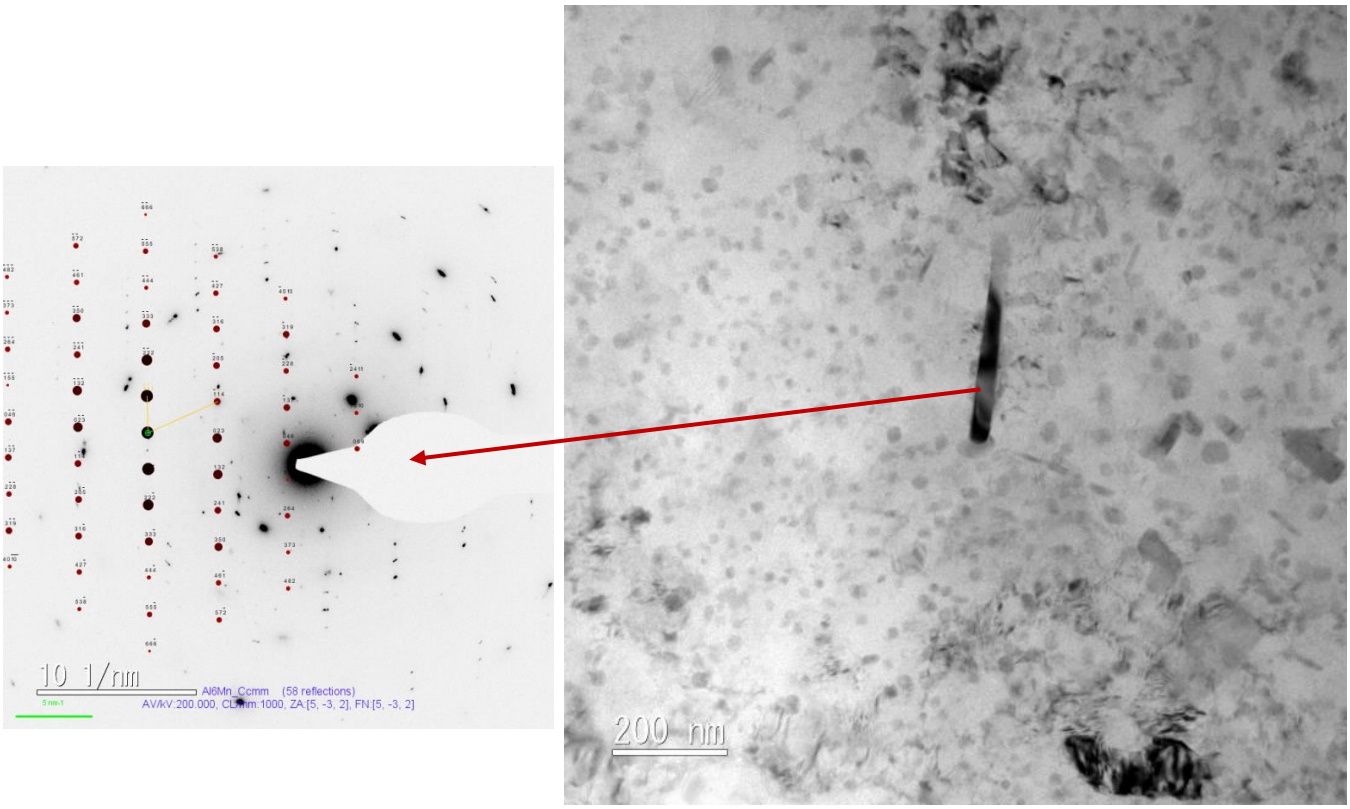

Figure 38 TEM bright filed with corresponding SAED pattern of pointed spot shows Al_6Mn

5.4.3.3 Small size precipitates

HR TEM image shows some areas which were occurred probably because of overlapping of grains or precipitates which causes Moire' patterns.

The average measured diameter for the small precipitations is 25nm.

Based on Fast Fourier Transformation (FTT) pattern, indexing phase is T'- and T- phase cannot be distinguished in terms of crystal structure.

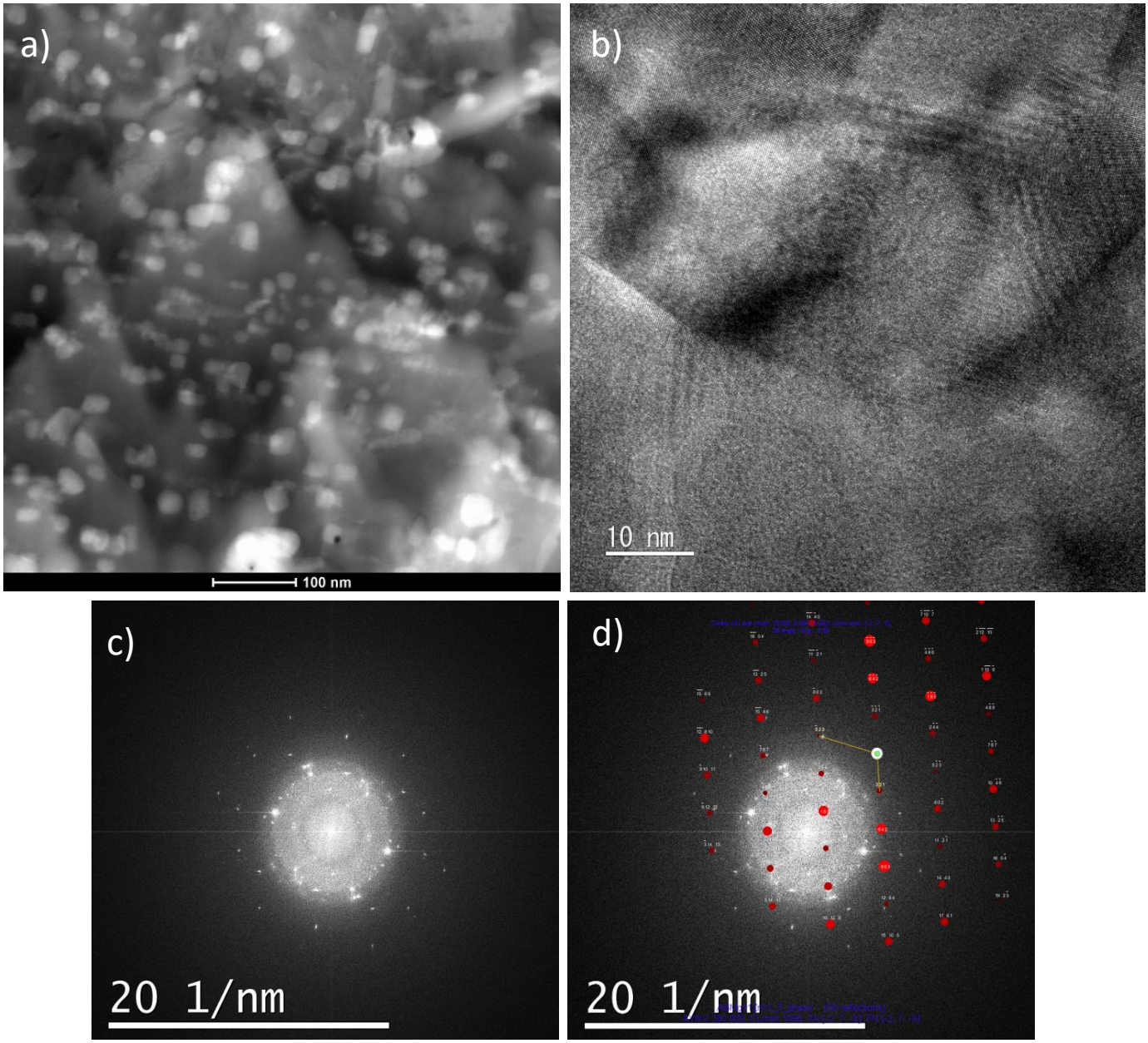

Figure 39 a) STEM HAADF image, b) HRTEM image, c)and d)Fast Fourier Transformation(FFT) image indexing T-phase of sample (3)

6 Discussion

In this chapter, the results of hardness measurements, DSC curves and TEM investigation are discussed.

6.1 Comparison of different heat treatment conditions on hardness of the alloy

According to the plotted hardness curve for three samples, it can be concluded that the sample (a) with pre-aging at 90°C for 24 hours followed by artificial aging at 140°C shows significant improvement of the hardness in compare to the sample (b) with single aging at 90°C and sample (c) with single aging at 140°C. Sample (a) shows pre-aging results in increasing peak hardness with decreasing the peak aging time. The hardness value of the sample (a) reaches the peak hardness in 40 hours after pre-aging.

It was also found the peak hardness in sample (b) and (c) with single step aging by increasing the temperature decreases, however in sample (b) with relatively low temperature no peak was observed during 500 hours and the hardness value showed rather increase within the aging. Sample (c) reaches the peak hardness after about 125 hours and then the over aging begins, which is the result of coarsening of the formed T-phase precipitates in the sample.

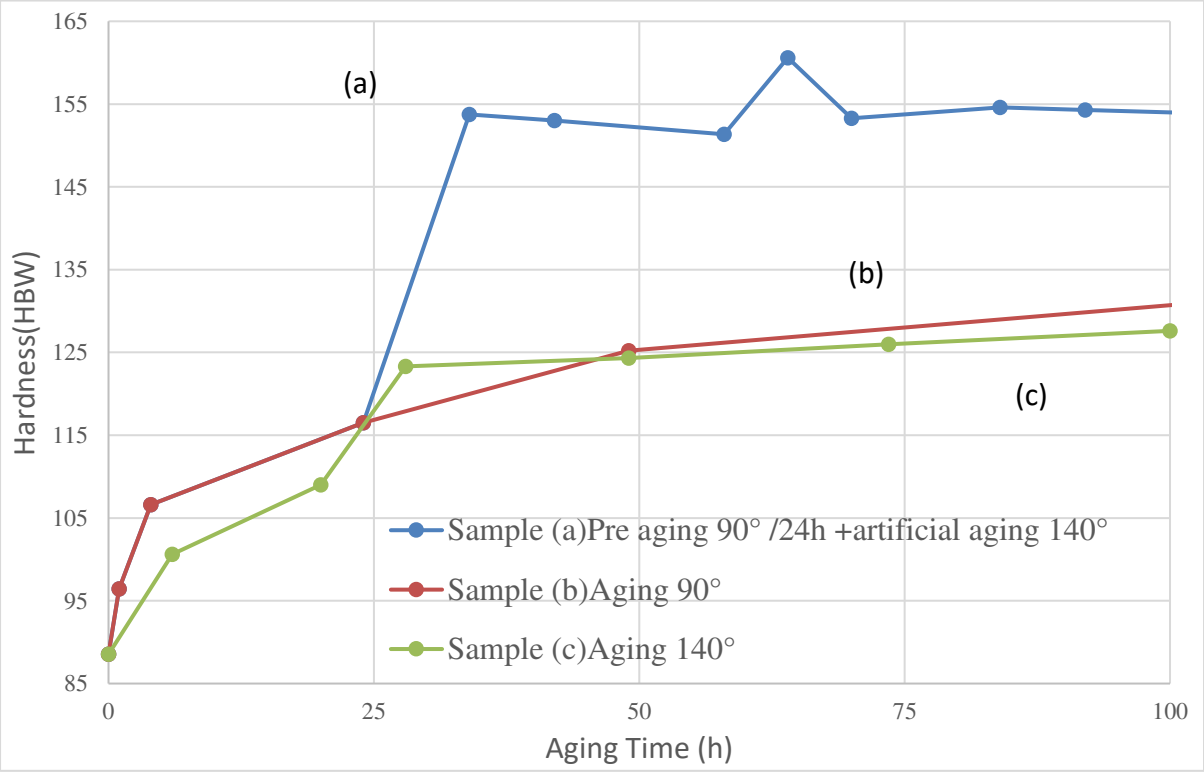

Figure 40 hardness value for different heat treatment conditions during 100 hours

According to the above experimental results, the alloy with chemical composition of Al-3.5Zn-5Mg-0.3Cu (wt %), shows a much better response to hardening by two steps heat treatment. Considering the hardness values of the three samples Figure 40 gives an over view of the hardness evolutions during the first 100 hours in sample (b) and (c) with single step aging in compare to sample (a) two steps aging. In Figure 40 also the sample with pre-aging shows much shorter time to reach the peak hardness.

6.2 Differential Scanning Calorimetry (DSC)

In Figure 41 the DSC run with heating rate of 10 K/min starts at approximately heat flow of 0 W/g at 25 °C and ends to about 0 W/g at 500°C due to the complete dissolution of all soluble phases in aluminium. The first three peaks correspond to the precipitation reaction and the last peak corresponds to the dissolution reaction.

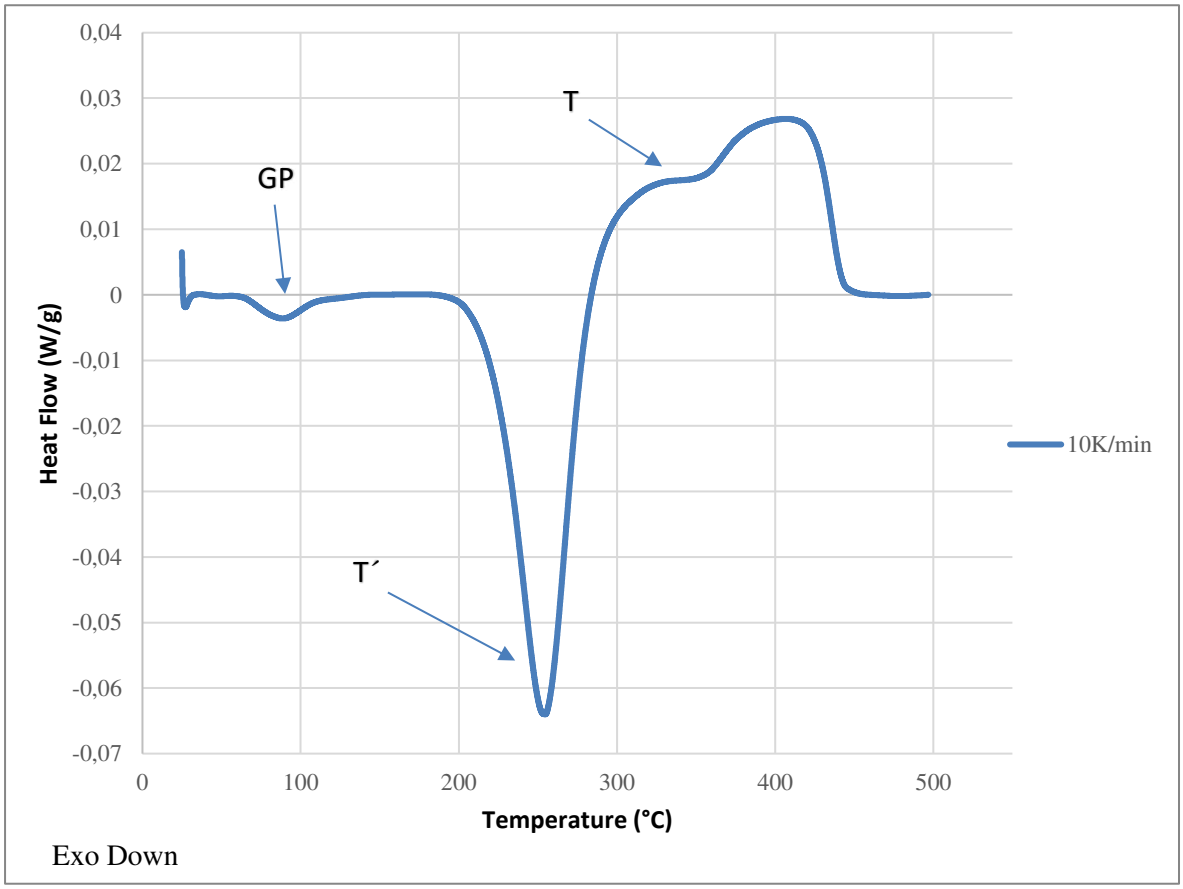

Figure 41 DSC run with heating rate of 10K/min

The first exothermic peak represents the formation of GP zone around 90°C, second peak represents T' which is around 250°C. Exothermal peak around 350°C is the transformation of T' to T phase. Next Peak is an endothermal peak around 400°C and represent dissolution of T.

The available DSC measurement exhibits the precipitation sequence as:

SSSS→ GP zone→ metastable phase T′→ equilibrium phase T [Al_{32} (Mg, Zn)$_{49}$]

The precipitation sequence with different heating rates are depicted in Figure 42. As the heating rate increase, the peaks shift to the higher temperatures and may results in overlapping or omitting some peaks. In order to prevent the peaks overlapping, lower heating rates were chosen for comparison. In figure below DSC runs with heating rates of 2, 5 and 10 K/min are demonstrated.

Exothermic reactions are in negative y-axis.

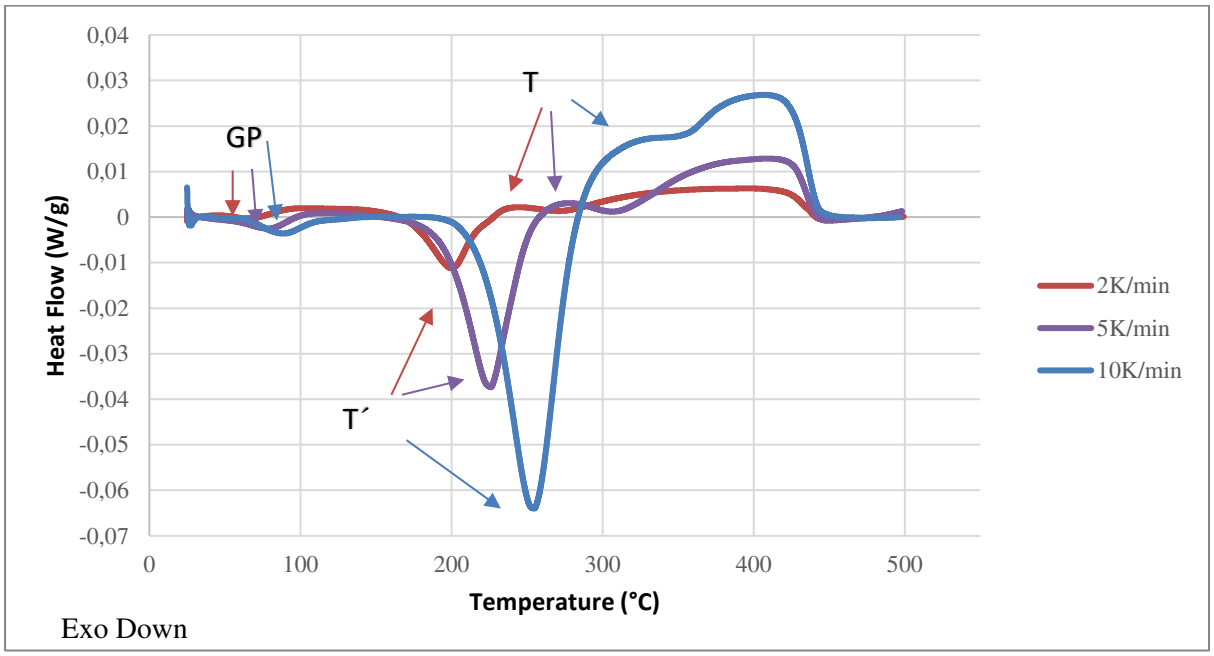

Figure 42 identification of precipitates with different heating rates

The first exothermic peak represents the formation of GP zone around 60-90°C, second peak represents T' which is around 200 to 250°C. Exothermal peak around 280 to 350°C is transformation of T' to T phase. Next Peak is an endothermal around 400-420°C and represent dissolution of T.

The hardness peak according to the DSC measurements can be explained by the fact that T'-phase is formed during aging.

6.3 Comparison of TEM results for different heat treatment condition

Three samples were prepared in order to investigate the crystallographic structure of the strengthening precipitates under TEM.

The selected samples (1) and (2) for TEM investigation were chosen during aging in order to detect the crystal structure of strengthening phase, which cause improvement in hardness of the material. The sample (1) were investigated after pre aging at 90 °C for 24 hours followed by aging at 140°C for 140 hours, which the hardness value is about 156 HBW and sample (2) after aging at 90°C for 500 hours with the hardness value of about 150 HBW. On the other hand, sample (3) was selected according to the obtained DSC curves around 275°C, where most probably T'-phase was formed in the sample.

TEM investigations on sample (1) and (2) show the crystal structure of the formed precipitates are T'- and T phases. As mentioned before, it was not possible for us to identify the difference between T- and T' precipitates in terms of crystal structure.

The detected precipitates in TEM investigations were categorised in three groups depending on their sizes:

- Large
- Medium
- Small

In all samples, large precipitates were distinguished as Mg_2Si and Al_6Mn on grain boundaries and for medium precipitates platelet shaped Al_6Mn or $Al_{18}Mg_6Mn_2$ in grains.

The small precipitates were identified as T-/T'-Precipitates in grains. In

Table 3 mean approximate diameter for small size T-/T'-Precipitates depending on the heat treatment of the samples are showed:

Sample	1	2	3
Mean diameter	10 nm	5 nm	25 nm

Table 3 T-/T'- precipitation mean diameter for the samples (1), (2) and (3)

It has to be noted, in samples (1) and (2) coherency between the matrix and the precipitates can be observed and these fine precipitates form obstacles to the motion of dislocations and improve the mechanical properties of the material.

Sample (3) shows no distinguished coherency between the matrix and the precipitates in HRTEM images and represent over aging state of the sample.

7 Summary and Conclusions

The hardening behavior of the alloy Al-3.5Zn-5Mg-0.3Cu (wt %), with higher Mg/Zn ratio in compare to 7xxx alloys, which was produced by gas metal arc welding (GMAW) in layer-by-layer manner, was investigated. As the production process and chemical composition of the alloy are different from conventional 7xxx aluminium alloys, investigation on age-hardening response of the alloy and the crystal structure of the formed precipitates were carried out.

The alloy hardness results show significant improvement during two steps aging. Material was preaged at 90° C for 24 hours followed by aging at 140° C for 622 hours in compare to single step aging, which one of them were aged at 90° C for 500 hours and the other one at 140 °C for 605 hours. Peak hardness decreases as temperature increases in the one-step artificial aging. Metallography was done in order to have an idea about the existing porosities in the produced alloy. Limited number of pores can be seen in the samples, but they can be almost considered as quasi pore- and crack-free manufactured parts for this kind of production method.

From DSC curves with different heating rates, the precipitation sequence can be interpreted as follows:

SSSS→ GP zone→ metastable phase T′→ equilibrium phase T [Al_{32} (Mg, Zn)$_{49}$]

The TEM investigations show the crystal structure of the formed precipitates based on Fast Fourier Transformation (FTT) pattern. The strengthening phase is probably T'-phase, which forms during aging and strengthen the material. Although the formed T'- and T- phase were not distinguishable from each other in terms of crystal structure.

8 References

[1] E. Herderick, " Additive manufacturing of metals: A review," *Materials science and technology 1413,* 2011.

[2] K. Cooper, "Rapid prototyping technology: selection and application," *CRC press,* 2001.

[3] J. Mehnen, J. Ding, H. Lockett and P. Kazanas, "Design study for wire and arc additive manufacture," *International Journal of Product Development,* vol. 19(1/2/3), pp. 2-20, 2014.

[4] D. Ding, Z. Pan, D. Cuiuri and H. Li, "Wire-feed additive manufacturing of metal components: technologies, developments and future interests," *The International Journal of Advanced Manufacturing Technology,* Vols. 81(1-4), pp. 465-481, 2015.

[5] D. Ding, Z. Pan, S. Van Duin, H. Li and C. Shen, "Fabricating superior NiAl bronze components through wire arc additive manufacturing," *Materials, ,* vol. 9(8), p. 652, 2016.

[6] J. Ding, P. Colegrove, J. Mehnen, S. Ganguly, P. Almeida, F. Wang and S. Williams, "Thermo-mechanical analysis of wire and arc additive layer manufacturing process on large multi-layer parts," *Computational Materials Science,* vol. 50(12), pp. 3315-3322, 2011.

[7] G. Lorenzin and G. Rutili, "The innovative use of low heat input in welding: experiences on 'cladding'and brazing using the CMT process," *Welding International,* vol. 23(8), pp. 622-632, 2009.

[8] J. L. Prado-Cerqueira, J. L. Diéguez and A. M. Camacho, "Preliminary development of a Wire and Arc Additive Manufacturing system (WAAM)," *Procedia Manufacturing,* vol. 13, pp. 895-902, 2017.

[9] M. Schnall, S. Bozorgi, T. Klein, R. Gradinger, A. Birgmann, P. Morais and P. Warzok, "Sonder-Aluminium-Schweißzusätze optimiert für die Verarbeitung im Wire-Arc Additive Manufacturing - Prozess".

[10] I. Polmear, D. StJohn, J. F. Nie and M. Qian, Light alloys: metallurgy of the light metals, Butterworth-Heinemann, 2017.

[11] J. R. Davis, Alloying: understanding the basics, ASM international, 2001.

[12] B. Sadler, Light metals 2013, Springer, 2017.

[13] E. Ghali, Corrosion resistance of aluminum and magnesium alloys: understanding, performance, and testing, John Wiley & Sons, 2010.

[14] A. P. Mouritz, Introduction to aerospace materials, Elsevier, 2012.

[15] A. Bhaduri, Mechanical Properties and Working of Metals and Alloys, Berlin: Springer, 2018.

[16] N. A. Belov, D. G. Eskin and A. A. Aksenov, Multicomponent phase diagrams: applications for commercial aluminum alloys, Elsevier, 2005.

[17] D. MacKenzie and G. Totten, Analytical characterization of aluminum, steel, and superalloys, CRC press, 2005.

[18] F. Ostermann, Anwendungstechnologie aluminium, 2015.

[19] H. Inoue, T. Sato, Y. Kojima and T. Takahashi, “The temperature limit for GP zone formation in an Al-Zn-Mg alloy,” *Metallurgical and Materials Transactions A,* vol. 12(8), pp. 1429-1434, 1981.

[20] S. Hou, P. Liu, D. Zhang, J. Zhang and L. Zhuang, “Precipitation hardening behavior and microstructure evolution of Al–5.1 Mg–0.15 Cu alloy with 3.0 Zn (wt%) addition,” *Journal of materials science,* vol. 53(5), pp. 3846-3861, 2018.

[21] S. Hou, D. Zhang, Q. Ding, J. Zhang and L. Zhuang, “Solute clustering and precipitation of Al-5.1 Mg-0.15 Cu-xZn alloy,” *Materials Science and Engineering: A, 759,* pp. 465-478, 2019.

[22] A. Bigot, P. Auger, S. Chambreland, D. Blavette and A. Reeves, “Atomic scale imaging and analysis of T'precipitates in Al-Mg-Zn alloys,” *Microscopy Microanalysis Microstructures, 8(2),* pp. 103-113, 1997.

9 List of figures

Figure 1 Schematic GMAW process layer-by-layer deposition [5] [4] 5
Figure 2 Main alloying elements in wrought alloy 7
Figure 3 Interstitial solid solution and high strained region within the crystal structure [14] 9
Figure 4 Subsitutional solid solution and high strained region in crystal structure [14] 10
Figure 5 Super saturated solid solution condition 12
Figure 6 GP1 zone toGP2 during aging [14] 13
Figure 7 Coherent precipitates structure [14] 13
Figure 8 Incoherent precipitates structure [14] 14
Figure 9 Strength and Particle size over the aging time [14] 14
Figure 10 Dislocation cutting through the particle [15] 15
Figure 11 Dislocation bypassing widely spaced particles [15] 16
Figure 12 relationship between strength and particle size for particles sheared (deformable particles) and particles by passed (non-deformable particles) by dislocations 16
Figure 13 the produced part by Gas Metal Arc Welding (GMAW) 20
Figure 14 Schematic sketch of heat treatment quenching furnace 21
Figure 15 Solution treatment, T4 condition of the samples 22
Figure 16 DSC for different heating rate 25
Figure 17 the three group of samples for Hardness measurements 26
Figure 18 cross section of the etched sample 28
Figure 19 DSC for the Alloy 29
Figure 20 DSC runs for different heating rates 30
Figure 21 Hardness Curves for the alloy during artificial aging at (a) 90° C for 24 h and subsequently aged at 140°C for 646 h, (b) 90° C for 500 h and, (c) 140° C for 605 h 31
Figure 22 Sample (1) and (2) 32
Figure 23 a) HAADF image and b)bright filed images of coarse secondary phase of sample 1 33
Figure 24 EDX analysis of STEM HAADF image show a) Mg_2Si and b) Al_6Mn 34
Figure 25 TEM bright field of medium size precipitates 35
Figure 26 EDX analysis of STEM HAADF image showing Al_6Mn 35
Figure 27 HRTEM image for sample 1 Fast Fourier Transformation(FFT) of sample 1 indexing T-Phase 36
Figure 28 a) STEM HAADF image and b) bright filed images of coarse secondary phase in the sample 2 37
Figure 29 EDX analysis of STEM HAADF image show a) Al_6Mn and b) Mg_2Si 37

Figure 30 TEM bright filed with corresponding SAED pattern of pointed spots show a) Mg_2Si and b) Al_6Mn. 38
Figure 31 EDX analysis of STEM HAADF image showing $Al_{18}Mg_3Mn_2$ 39
Figure 32 TEM bright filed with corresponding SAED pattern of pointed spot shows Al_{18} Mg_3Mn_2 39
Figure 33 a) TEM bright field b) HRTEM image c)Fast Fourier Transformation(FFT) image of sample (2) 40
Figure 34 a)STEM HAADF image and b)bright filed images of coarse secondary phase of sample (3) 40
Figure 35 EDX analysis of STEM HAADF image showing Al_6Mn 41
Figure 36 TEM bright filed with corresponding SAED pattern of pointed area shows Al_6Mn 41
Figure 37 EDX analysis of STEM HAADF image showing Al_6Mn 42
Figure 38 TEM bright filed with corresponding SAED pattern of pointed spot shows Al_6Mn 42
Figure 39 a) STEM HAADF image, b) HRTEM image, c)and d)Fast Fourier Transformation(FFT) image indexing T-phase of sample (3) 43
Figure 40 hardness value for different heat treatment conditions during 100 hours 44
Figure 41 DSC run with heating rate of 10K/min 45
Figure 42 identification of precipitates with different heating rates 46

10 List of tables

Table 1 Crystal structure of metastable phases formed in commercial alloys of the Al-Cu-Mg-Zn system [16] *17*

Table 2 Nominal chemical compositions (wt%) of the alloy *19*

Table 3 T-/T'- precipitation mean diameter for the samples (1),(2) and (3) *47*